AD_____

Award Number: DAMD17-98-1-8251

TITLE: Understanding the Role of Replication Protein A and RAD52 in Breast Cancer

PRINCIPAL INVESTIGATOR: Gloria Borgstahl, Ph.D.

CONTRACTING ORGANIZATION: The University of Toledo
Toledo, Ohio 43606-3390

REPORT DATE: October 2001

TYPE OF REPORT: Annual

PREPARED FOR: U.S. Army Medical Research and Materiel Command
Fort Detrick, Maryland 21702-5012

DISTRIBUTION STATEMENT: Approved for Public Release;
Distribution Unlimited

The views, opinions and/or findings contained in this report are those of the author(s) and should not be construed as an official Department of the Army position, policy or decision unless so designated by other documentation.

20020124 369

REPORT DOCUMENTATION PAGE

Form Approved
OMB No. 074-0188

Public reporting burden for this collection of information is estimated to average 1 hour per response, including the time for reviewing instructions, searching existing data sources, gathering and maintaining the data needed, and completing and reviewing this collection of information. Send comments regarding this burden estimate or any other aspect of this collection of information, including suggestions for reducing this burden to Washington Headquarters Services, Directorate for Information Operations and Reports, 1215 Jefferson Davis Highway, Suite 1204, Arlington, VA 22202-4302, and to the Office of Management and Budget, Paperwork Reduction Project (0704-0188), Washington, DC 20503

1. AGENCY USE ONLY (Leave blank)	2. REPORT DATE October 2001	3. REPORT TYPE AND DATES COVERED Annual (25 Sep 00 - 24 Sep 01)

4. TITLE AND SUBTITLE
Understanding the Role of Replication Protein A and RAD52 in Breast Cancer

5. FUNDING NUMBERS
DAMD17-98-1-8251

6. AUTHOR(S)
Gloria Borgstahl, Ph.D.

7. PERFORMING ORGANIZATION NAME(S) AND ADDRESS(ES)
The University of Toledo
Toledo, Ohio 43606-3390

E-Mail: gborgst@uoft02.utoledo.edu

8. PERFORMING ORGANIZATION REPORT NUMBER

9. SPONSORING / MONITORING AGENCY NAME(S) AND ADDRESS(ES)

U.S. Army Medical Research and Materiel Command
Fort Detrick, Maryland 21702-5012

10. SPONSORING / MONITORING AGENCY REPORT NUMBER

11. SUPPLEMENTARY NOTES

12a. DISTRIBUTION / AVAILABILITY STATEMENT
Approved for Public Release; Distribution Unlimited

12b. DISTRIBUTION CODE

13. ABSTRACT *(Maximum 200 Words)*

This research focuses on structural studies of human replication protein A (RPA) and RAD52 in recombination-based repair of double-stranded DNA breaks. This DNA repair pathway has been directly linked to breast cancer through BRCA1 and BRCA2 protein-protein interactions. Also, mutations in the ataxia telangiectasia (AT) gene are implicated in breast cancer and recently AT kinase was shown to phosphorylate the N-terminus of the 32 kDa subunit of RPA. The goals of the Borgstahl laboratory are to understand the role of RPA phosphorylation and RPA/RAD52 protein-protein interactions in DNA repair. The ultimate goal of this research is to provide an understanding of this process at the atomic level.

14. SUBJECT TERMS
Breast Cancer

15. NUMBER OF PAGES
32

16. PRICE CODE

17. SECURITY CLASSIFICATION OF REPORT Unclassified	18. SECURITY CLASSIFICATION OF THIS PAGE Unclassified	19. SECURITY CLASSIFICATION OF ABSTRACT Unclassified	20. LIMITATION OF ABSTRACT Unlimited

NSN 7540-01-280-5500

Standard Form 298 (Rev. 2-89)
Prescribed by ANSI Std. Z39-18

Table of Contents

1. Abstract for poster presentation: V. Kabaleeswaran and G. E. O. Borgstahl "Structural studies on full-length human replication protein A heterodimer", ACA National Meeting (V) Los Angeles, CA, July 2001.

2. Abstract for Talk: Doba Jackson and G. Borgstahl, "Characterization of the Human RAD52wt and RPA Protein protein Interaction", Sigma Xi Scientific Research Society (V), Toledo, OH April 20, 2001.

3. Abstract for Talk: Wasantha Ranatunga and G. Borgstahl, "Human Rad52 Protein has Extreme Thermal Stability", Sigma Xi Scientific Research Society (V), Toledo, OH April 20, 2001.

4. Reprint of publication: Habel, J. E., Ohren, J. F. and Borgstahl, G. E. O. "Dynamic light scattering analysis of full-length, human RPA14/32 dimer: purification crystallization and self-association" *Acta Cryst.* **D57**, 254-259 (2001).

5. Reprint of publication: Ranatunga, W., Jackson, D., Lloyd, J. A., Forget, A. L., Knight, K. L. and Borgstahl, G. E. O. "Human Rad52 Exhibits Two Modes of Self-association" *J. Biol. Chem.* **276**, 15876-15880 (2001). *Accepted without revision.*

6. Reprint of publication: Ranatunga, W., Jackson, D., Flowers II, R. A. and Borgstahl, G. E. O. "Human Rad52 Protein Has Extreme Thermal Stability" *Biochemistry* **40**, 8557-8562 (2001).

Introduction

This is the third year report for my four-year Career Development Award (CDA) and my three-year IDEA award. These two awards have been combined under one award number (DAMD17-98-1-8251) and this report describes the progress made for both awards.

Introduction to the project

This research focuses on structural studies of human replication protein A (RPA) and RAD52. RPA is a central molecule of the molecular machinery of DNA metabolism and is essential for DNA replication, recombination and repair [15]. RPA interacts specifically with RAD52 [10] and is involved in the early stages of recombination-based repair of double-stranded DNA breaks [12]. This DNA repair pathway has been directly linked to breast cancer through BRCA1 and BRCA2 protein-protein interactions [1]. Mutations in the ataxia telangiectasia (AT) gene are also implicated in breast cancer [8] and recently AT kinase was shown to phosphorylate threonine and serine residues of the 32 kDa subunit of RPA [6]. The goals of the Borgstahl laboratory are to understand the role of RPA phosphorylation and RPA/RAD52 protein-protein interactions in DNA repair. The ultimate goal of this research is to provide an understanding of this process at the atomic level. Towards this aim constructs of RPA, RAD52 and the RPA/RAD52 complex that are suitable for crystallization will be found and then crystallized for structure determination by X-ray crystallography.

Development of a breast cancer focus in my lab

The purpose of the CDA was to provide me with the additional time and support needed to establish a structural biology laboratory with a focus on the protein-protein and protein-DNA interactions involved in double-strand break repair. Upon the award of the CDA the chair of our department relieved me of my formal teaching responsibilities (which constituted 40% of my effort) in order to permit me to focus my efforts on breast cancer research. I continued, during the course of the year, to train graduate students. This training includes an informal special topics course in protein crystallography. Seven graduate students and a technician have been involved in getting this program off the ground. Three of the students (Jeff Ohren, Krishnamurthy Rajeswari and Cathy Schellert) received M.S. degrees for their efforts in the summer of 1999. Jeff worked on the purification and crystallization of RPA and Rajee and Cathy worked on creating and characterizing the domain constructs of RAD52 protein. The other four are Ph.D. students and are working on various aspects of this project for their doctorate. Since the funding of the CDA award I have been able to wok side-by-side in the laboratory with my students. This year we have created new constructs, developed new techniques, learned new methodologies, grown protein crystals and collected high quality synchrotron diffraction data to achieve the technical objectives of this award.

Body

Changes to the statement of work objectives from the original proposal were explained in the progress report for the period 25-Sep-98 – 24-Sep-99 and will not be repeated here. In that report objective 1 was abandoned and objective 2 was completed. Progress on objectives 3 and 4 are described in this report. The text of the objective

has been copied and below each objective the tasks which have been completed are described. When appropriate any changes that have occurred are explained and how the project will proceed in the next year of this award is explained.

Objective 3: *Identify regions of RPA that interact with RAD52.*

Regions on the C-terminal domain of RPA32 and midsection of RPA70 have been identified as interacting with RAD52 in the previous reports. Functional assays are expected to help decipher these results. Recently we have found that Rad52 binding to RPA increases the DNA affinity of RPA. We have also found that binding by RPA disrupts the higher order self-association of Rad52. These results have mechanistic implications in double strand break repair and together with our previously reported ELISA protein-protein interaction results are being prepared for publication.

A collaboration was established last year with Dr. Kendall Knight at the University of Massachusetts to study the aggregation state of RAD52. Results were described in the report from last year. This year these results were written up and published in the Journal of Biological Chemistry. This manuscript by Ranatunga *et al.* (2001) is included in the appendices.

In the report from last year we also reported results on differential scanning calorimetry data on wild-type and mutant Rad52. Wild-type and mutant hRad52 data showed that the wild-type protein has extreme thermal stability (T_M 115 °C). The N-terminal half is responsible for ring formation and the C-terminal half participates in the higher order self-association of rings. This work was written up and published in Biochemistry this year. This manuscript by Ranatunga *et al* (2001) is included in the appendices. The abstracts for two talks presented at a local Sigma Xi conference by my students are also included in the appendix.

Although scRad52 has similar activity and forms ring structures, the C-terminal half of the protein has only 18% sequence identity with hRad52 and yeast proteins can not substitute for human proteins in activity assays. The higher order self-association and thermal stability of wild-type and mutant forms of scRad52 will be studied and compared to hRad52. The thermal stability and thermodynamic properties of the RPA:Rad52 complex will be measured.

Objective 4: *Test the feasibility of crystallizing the phosphorylated proteins obtained in objectives 1 and 2 and perform crystallization trials on the proteins obtained in objective 3.*

Several soluble active fragments (SAF) of RAD52 have been obtained for crystallization. Crystallization efforts have been continuously underway this year with no reportable outcomes, yet. Of brighter note, several crystal forms of RPA heterodimer have been grown in four different space groups and excellent diffraction data collected at the synchrotron. A manuscript reporting the use of dynamic light scattering to promote crystallization and to study the self association of RPA14/32 has been been published in Acta Crystallographica D. A reprint of this manuscript is included in the appendix of this report. One abstract of a poster presentation by my postdoctoral fellow at the national American Crystallographic Association conference is also included in the appendix.

Significance – first RPA14/32 structure. The crystal structure of human RPA14/32 will reveal for the first time the structure of the intact RPA32 subunit,

including the N-terminus, which is hyperphosphorylated during apoptosis and in response to DNA damage, and the C-terminal domain, which interacts with several DNA metabolic proteins, including Rad52. Comparison of this structure with that of the already determined proteolytic core of RPA14/32 (protein data bank entry 1QUQ) will reveal why the core binds ssDNA weakly while the intact protein does not bind ssDNA [2].

A combination of two phasing methods, molecular replacement and multi-wavelength anomalous dispersion (MAD), are being used to solve the phase problem for the first structure of RPA14/32 [7]. As soon as the first native diffraction data on RPA14/32 were collected, extensive attempts to solve the structure by molecular replacement using the coordinates of RPA14(3-116)/RPA32(45-170) from the protein data bank (entry 1QUQ) were made. Solutions were found and in some cases, weak density for the missing domains could be seen. However, phasing was never sufficient to produce clean maps that could be reliably interpreted for the missing domains. All attempts on all crystal forms failed. There are three possible reasons for this. Entry 1QUQ provides only 56% of the structure in the crystals. RPA14(3-116) and RPA32(45-170) are structurally very similar (see Fig. 4 and Fig. 2 in Bochkarev et al. (1999)) and molecular replacement may put 14 where 32 belongs and vice versa. Finally, perhaps the structure of the full-length RPA14/32 differs from the protease resistant core. Ambiguity between the hexagonal space groups and number of molecules in the asymmetric unit was also a problem.

Excellent progress on the structure determination of RPA14/32 has been made since the first submission of this application to the ACS. Two MAD datasets had already been collected (Fig. 1A,B). The first crystals were of a selenomethionine (SeMet) derivative [5]. Only the hexagonal crystal form can be grown when RPA14/32 contains SeMet. This crystal showed textbook quality Se fluorescence; diffracted to 2.5 Å resolution and four wavelength MAD diffraction data were collected at the IMCA-CAT at the Advanced Photon Source (Fig. 1A). Unfortunately, the data were collected at a close crystal-to-detector distance in order to obtain 2.5 Å resolution data and caused the diffraction spots to be too closely spaced on the images. The instrument configuration was corrected and the data recollected but these data though sufficiently redundant only extend to 3.0 Å resolution. There was not enough remaining beamtime to put on a second crystal. The 2.5 Å data could not be processed with standard software (HKL2000) due to the close spacing of the spots. New software, developed to process data with these types of problems (PrOW) was installed and successfully integrated the data [3]. An anomalous difference Patterson map for the SeMet data collected at the peak wavelength showed Se sites (Fig. 1A). We also have collected bromine (Br) MAD diffraction data on a hexagonal crystal of RPA14/32at Stanford Synchrotron Radiation Laboratory beamline 9-2. The crystal was soaked in 1 M NaBr for one minute and then cryocooled following published methods [4]. The use of Br MAD phasing is a relatively new technique. Complete anomalous diffraction data were collected at wavelengths corresponding to the peak and edge of the bromine fluorescence. The anomalous difference Patterson map calculated at 2.4 Å resolution shows ordered Br sites in the crystal (Fig. 1B).
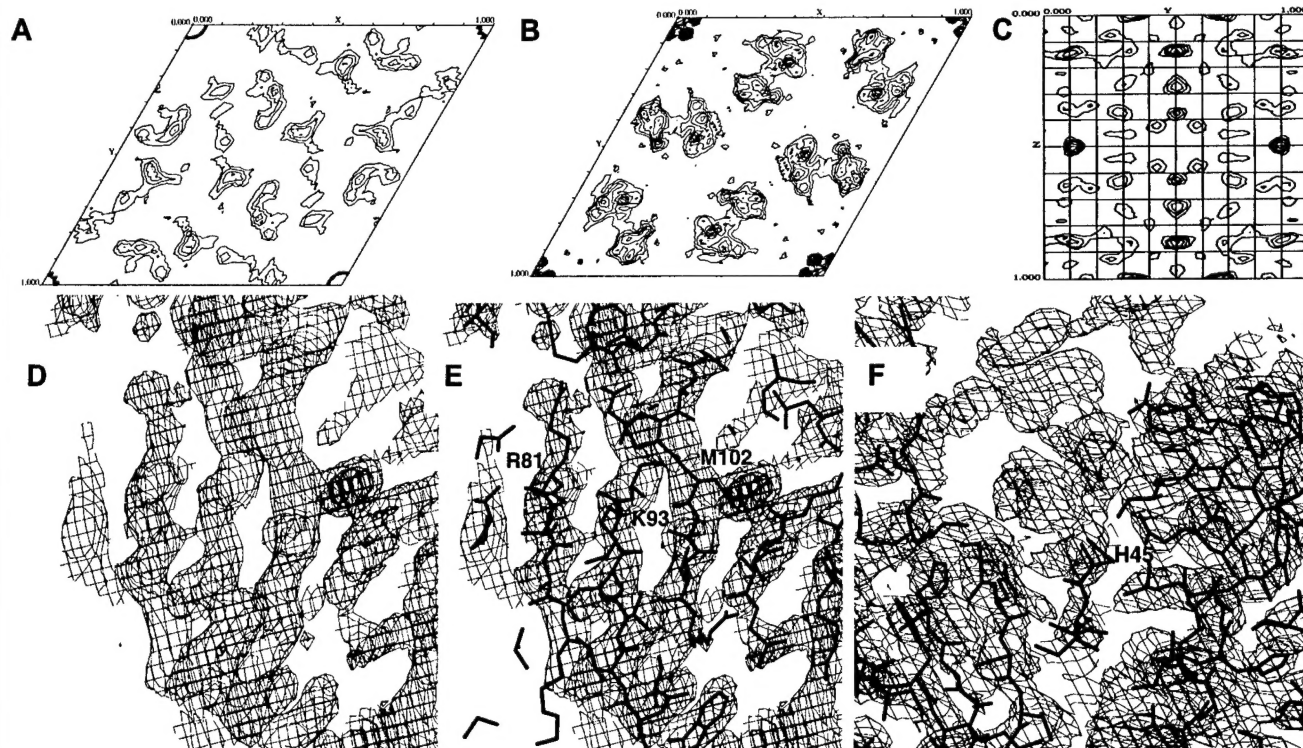
Fig. 1. Progress towards phasing hexagonal and orthorhombic crystals of full length human RPA14/32. Anomalous difference Pattersons for **(A)** hexagonal SeMet derivative calculated at 3.5 Å resolution, **(B)** cryocooled NaBr soaked hexagonal crystals calculated at 2.4 Å resolution. **(C)** platinum derivative for orthorhombic form I crystals. SAD Electron density maps for **(D)** 3 β-strands with a Met indicated by the strong selenium peak (3 Å resolution, thin cages are contoured at 1σ, and thick 5σ). Map was calculated as spacegroup p6₅ phased with phases from the initial 16 Se sites found by SHELXD, phase refinement by SHARP (FOM=0.33), and 60% solvent flattening and NCS averaging by RESOLVE (FOM = 0.53). **(E)** The same section with the corresponding region of RPA32 atomic model superimposed (heavy lines). Labels indicate the positions of Arg81, Lys93 and Met102. **(F)** Density corresponding to the N-terminal domain of RPA32 (phased from 20 Se, peak anomalous data only, 25% solvent, NCS averaged; FOM=0.62, 3 Å resolution, 1σ contours). Again the atomic model of the RPA14/32 core is drawn with heavy lines. RPA32 residue His45 is labeled in the center of the figure.

The licenses for several new software packages have been obtained in the last 3 months and installed to solve the RPA14/32 phase problem. Initially only one heterodimer per asymmetric unit was assumed and so only the top 16 Se sites found by SHELXD in the 2.5 Å Se peak data were refined with SHARP using the single anomalous dispersion or SAD method [14]. Then RESOLVE was used to find the noncrystallographic symmetry (NCS) axes based on the Se positions, to perform maximum likelihood refinement of the phases and reciprocal space solvent flattening with 60% solvent [13]. The resulting SAD Fourier map, with the Met positions, was easily interpreted (Fig. 1D & 1E). Surprisingly not one but two RPA14/32 proteolytic core molecules were placed in the density by hand using the computer graphics

program XFIT [9]. This partial model comprises 56% of the total structure ([229 out of 410 possible residues]X2) and has been refined with CNS software and simulated annealing to a crystallographic R value of 29.5% (R_{free} 36.5%). Analysis of the residual density by SHARP has found 4 more Se sites, density for the missing regions of RPA32 using SAD phasing from 20 Se positions are shown in Fig. 1F. Analysis of the remaining Se sites with SHARP is in progress as this grant application is being written. Upon completion of the Se model, the phases will be improved by combining the Se peak data with the rest of the MAD data. Then the Br sites will be located using the Se phases and phase combination will be performed with SHARP. Preliminary results, using the easy to use but less powerful software XHEAVY, indicate that combination of the Br data with the Se data in this manner increases the figure of merit (FOM) of the phases by at least 0.15. The very best phases will then be obtained by combining the Se/Br phases with calculated phases from the refined model of the protein core using SIGMAA [11]. Then we will finish tracing the main chain of the remaining N- and C-terminal domains of RPA32, the 109-119 loop of RPA32 and a few residues of RPA14. Reasonable electron density is already visible for these regions (Fig. 1F) and it is expected to continue to improve as the phasing improves and the resolution is extended. In hindsight, these crystals were quite robust when handled, which we now know to be due to their low solvent content of 30.1%. The structure from this crystal form is expected to be well ordered with little room for excessive domain movements.

Purification of several RPA and Rad52 constructs are underway and summarized in the table below. Crystallization screening will continue into the last year of this award.

Table 1. Proteins targeted for crystallization and dynamic light scattering measurements made to date

Protein	Conc. mg/ml	R_H nm	C_P nm	C_P/R_H %	Baseline	modality	S.O.S error
1. scRPA14/32	10	3.79	0.67	17.7	1.000	mono	0.658
2. hRPA14/32(8Asp)	4.0	3.46 (85%)	na	na	1.003	Bi	0.750
3. htRPA +10 mM DTT	5.5	5.9 (93.9%)	na	na	1.004	Bi	1.97
4. htRPA + 10 mM DTT + 10 mM MgCl$_2$	10	5.67	1.0	17.9	1.001	mono	1.12
5. sctRPA+ 10 mM DTT + 5 mM MgCl$_2$	2.3	5.71	1.4	24.9	0.999	mono	3.44
6. htRPA(8Asp)	7.0	5.6	0.7	12.3	1.000	mono	1.54
7. hRad52 + HGP	3.5	6.6 (10.5%) 27.6 (85.8%)	na	na	1.007	multi	3.10
8. hRad52 + HGP + heat step after lysis	3.5	14.7	4.2	28.8	1.001	mono	4.20
9. hRad52(1-192)	15	6.1	1.3	21.4	1.001	mono	1.95
10. hRad52(218-418)	3.3	6.5	2.2	34.2	1.001	mono	2.59
11. hRad52(218-418), pH 10	4.0	6.5	0.8	12.6	1.000	mono	2.59
12. RPA:Rad52(218-418)	1.2	5.05	0.8	16.2	1.001	mono	9.83

n.a. not applicable. Monomodal statistics are from Dynamics and bimodal distributions were analyzed with DynaLS software to remove contributions from solvent or large aggregates.

Key Research Accomplishments

- Solved of the crystallographic phase problem for crystals of full length human RPA14/32.
- Constructs of phosphorylation mutant of heterotrimeric and dimeric human RPA and yeast RFA were purified and screening for crystallization has begun.
- Purified several mutant RPA and RAD52 mutants for examination of the role of RPA/RAD52 interaction in activity.

Reportable Outcomes

Manuscripts, abstracts, presentation (attached in appendix):

- Poster presentation: V. Kabaleeswaran and G. E. O. Borgstahl "Structural studies on full-length human replication protein A heterodimer", ACA National Meeting (V) Los Angeles, CA, July 2001.

- Talk: Doba Jackson and G. Borgstahl, "Characterization of the Human RAD52wt and RPA Protein protein Interaction", Sigma Xi Scientific Research Society (V), Toledo, OH April 20, 2001.

- Talk: Wasantha Ranatunga and G. Borgstahl, "Human Rad52 Protein has Extreme Thermal Stability", Sigma Xi Scientific Research Society (V), Toledo, OH April 20, 2001.

- Publication: Habel, J. E., Ohren, J. F. and Borgstahl, G. E. O. "Dynamic light scattering analysis of full-length, human RPA14/32 dimer: purification crystallization and self-association" *Acta Cryst.* **D57**, 254-259 (2001).

- Publication: Ranatunga, W., Jackson, D., Lloyd, J. A., Forget, A. L., Knight, K. L. and Borgstahl, G. E. O. "Human Rad52 Exhibits Two Modes of Self-association" *J. Biol. Chem.* **276**, 15876-15880 (2001). *Accepted without revision.*

- Publication: Ranatunga, W., Jackson, D., Flowers II, R. A. and Borgstahl, G. E. O. "Human Rad52 Protein Has Extreme Thermal Stability" *Biochemistry* **40**, 8557-8562 (2001).

Research Proposal activity

- "Structural Studies on Replication Protein A" Borgstahl PI submitted to American Cancer Society 4/1/01, Total budget **$936,506** for 4 years. Ranked 7/51 but only 6 were funded! The application was updated and resubmitted 10/15/01.

- "Structural Studies on Replication Protein A and Rad52" Borgstahl PI. Submitted as an R01 application to the NIH 2/1/01, Total budget **$1,263,930** for 5 years. Under revision for 3/1/02 resubmission.

Conclusions

Protein-protein interactions between RPA and RAD52 are important in the first step of the double-strand break repair pathway. RPA is phosphorylated in a cell-cycle dependent manner and by several enzymes *in vitro* including AT kinase. The role of RPA phosphorylation is not well understood, but it does not appear to modulate the interaction of RPA with RAD52. Interestingly, RPA phosphorylation has recently been shown to promote the dissociation of RPA14/32 dimer from the RPA70 subunit. In the

next 2 years of this award the structural consequences of phosphorylation on RPA structure will be investigated in the context of the RPA heterotrimer and the dimer. Mutation of Thr and Ser to Asp will be used to mimic phosphorylation. To date, only proteolytically stable core fragments of RPA have been crystallized and their structures solved. During year 1 of this award the full-length RPA14/32 dimer was crystallized in two crystal forms, many sets of X-ray diffraction data were collected and the structure will be solved in the second year of this award. RAD52 was been found to aggregate in solution and electron micrograph studies show that it forms ring structures in solution. These aggregates are polydisperse with 8-10 monomers per ring and multiple rings can associate to form higher molecular weight aggregates. Such aggregation has been problematic for crystallization. Fortunately, we have found several suitable constructs that are soluble and retain single-stranded DNA binding and/or RPA binding activities. During year 2, the crystallization of RPA14/32 was further extended and more data was collected and a manuscript concerning this work was published. Constructs for expression of yeast RFA14/32 and a phosphorylation mimic of human RPA14/32 were created. Dynamic light scattering data and electron micrographs and have delineated the roles of the N- and C-terminal halves of RAD52 in ring formation and super ring aggregation. Differential scanning calorimetry data demonstrated the extreme thermal stability of RAD52 and stimulated new ideas on how to crystallize and purify RAD52. Crystallization trials for all constructs discussed are continuing. Structural determination of these proteins by X-ray crystallography will reveal a wealth of information on how they function in double-strand break repair. In year 3 several manuscripts were prepared and published. Key information on the effect of Rad52 binding to RPA on ssDNA affinity and Rad52 self-association were made. The crystallographic phase problem for human RPA14/32 was solved.

References

1. Bertwistle, D. and A. Ashworth, *Functions of the BRCA1 and BRCA2 genes.* Curr. Opin. Genet. Dev., (1998). **8**, 14-20.
2. Bochkareva, E., L. Frappier, A.M. Edwards and A. Bochkarev, *The RPA32 Subunit of Human Replication Protein A Contains a Single-stranded DNA-binding Domain.* J. Biol. Chem., (1998). **273**, 3932-3936.
3. Bourgeois, D., *New processing tools for weak and/or spatially overlapped macromolecular diffraction patterns.* Acta Cryst., (1999). **D55**, 1733-1741.
4. Dauter, Z., M. Dauter and K.R. Rajashankar, *Novel approach to phasing proteins: derivatization by short cryo-soaking with halides.* Acta Cryst., (2000). **D56**, 232-237.
5. Doublie, S., *Preparation of selenomethionyl proteins for phase determination.* Methods Enzymol., (1997). **276**, 523-530.
6. Gately, D.P., J.C. Hittle, G.K.T. Chan and T.J. Yen, *Characterization of ATM Expression, Localization and Associated DNA-dependent Protein Kinase Activity.* Mol. Biol. Cell, (1998). **9**, 2361-2374.
7. Hendrickson, W.A. and C.M. Ogata, *Phase Determination from Multiwavelength Anomalous Diffraction Measurements.* Methods Enzymol., (1997). **276**, 494-523.
8. Lavin, M., *Role of the ataxis-telangiectasia gene (ATM) in breast cancer.* BMJ, (1998). **317**, 486-487.
9. McRee, D.E., *Practical Protein Crystallography.* 1993, San Diego, CA: Academic Press, Inc.
10. Park, M.S., D.L. Ludwig, E. Stigger and S.H. Lee, *Physical interaction between Human RAD52 and RPA is Required for Homologous Recombination in Mammalian Cells.* J. Biol. Chem., (1996). **271**, 18996-19000.
11. Read, R.J., *Model phases: Probabilities and bias.* Methods Enzymol., (1997). **277**, 110-128.
12. Shinohara, A. and T. Ogawa, *Homologous recombination and the roles of double-strand breaks.* Trends Biochem Sci, (1995). **20**, 387-391.
13. Terwilliger, T.C., *Maximum-likelihood density modification.* Acta Cryst., (2000). **D56**, 965-972.
14. Terwilliger, T.C. and J. Berendzen, *Automated structure solution for MIR and MAD.* Acta Cryst., (1999). **D55**, 849-861.
15. Wold, M.S., *RPA: A Heterotrimeric, Single-Stranded DNA-Binding Protein Required for Eukaryotic DNA Metabolism.* Ann. Rev. Biochem., (1997). **66**, 61-91.

Structural studies on full-length human replication protein A heterodimer

Venkataraman Kabaleeswaran and Gloria Borgstahl

Department of Chemistry, The University of Toledo, 2801 W. Bancroft Street, Toledo, OH 43606

Human replication protein A (RPA) is a single stranded DNA binding protein, which plays a major role in DNA replication, DNA-repair and recombination. It exists in two forms as heterotrimer with three subunits of 70, 32 and 14 kDa and heterodimer of two subunits 32 and 14 kDa. The heterodimer is known to separate from the heterotrimer upon apoptotic phosphorylation. The heterodimer contains a protein-protein interaction, DNA binding and phosphorylation domain. The structure of a protease resistant core of RPA heterodimer has been solved. The DNA binding properties and the mode and role of phosphorlyation has not been established clearly. The function of human RPA heterodimer is still not well understood due to the lack of a complete structure. In order to contribute to the functional understanding of the heterodimer, we have focused on solving the complete structure of RPA heterodimer. Native data were collected at SSRL beam line 7-1. Initial efforts to solve this structure by molecular replacement failed. Therefore, four wavelength MAD data were collected at APS on a selenomethionyl derivative at 3.0 Å and initial phases were obtained from 12 selenium sites using SOLVE. In order to improve the phases further, two wavelength MAD data at 2.5 Å resolution were collected on a NaBr derivative at SSRL beam line 9-2. Bromine sites were obtained using SOLVE and attempts are being made to combine both phase sets to solve the structure. Up to date results on the structure solution will be presented.

Characterization of the human Rad52wt and RPA protein-protein interaction

Doba Jackson

Advisor- Gloria Borgstahl

Department of Chemistry, ext. 1581, djackso2@uoft02.utoledo.edu

Double-strand breaks (DSB's) in DNA are a direct result of ionizing radiation. The human Rad52 and RPA proteins play an important role in the earliest stages of chromosomal double-stranded break repair via the homologous recombination pathway. The protein-protein interactions between Rad52 and RPA are well established with both yeast and human proteins (1,2). Rad52 and RPA both have been found to stimulate homologous recombination *in vitro*. The stimulation by RPA has been found to have two components. The first is to remove secondary structure from ssDNA. The second component is to interact specifically with other proteins relieving of secondary structure of ssDNA. The second component involves making specific protein-protein contacts with Rad52 and Rad51 (3).

The presented work will describe the molecular characterization of Rad52 and RPA interaction using a modified enzyme-linked immunosorbant assay (ELISA), immunoprecipitation, dynamic light scattering (DLS) and static light scattering (SLS). The Rad52 binding site for RPA32 was previously established to reside between residues 221-280 on Rad52, which has been, established as a RPA 32 kDa subunit (RPA32) binding domain (1). The RPA 70 kDa subunit (RPA70) binding site on Rad52 was not established in the previous study. Here I describe a c-terminal deletion mutant of Rad52 (amino acids 218-418) that carries both binding sites of RPA70 subunit and RPA32 subunit. Activity of the mutant Rad52 is similar to wild-type in binding RPA. Also, the solution properties of mutant Rad52 exhibits the high-order aggregation properties of the wild-type Rad52 without forming a heptameric ring-structure (5). The Rad52 binding site on RPA was investigated and found to reside on amino-acid residues 224 to 271 on RPA32 subunit and residues 168-326 on RPA70 kDa subunit. The RPA32 interaction appears to be mediated by electrostatic interactions similar to other protein interactions with RPA32 such as XPA and UNG1 (4). The RPA70 interaction resides in the domain, which is known to bind ssDNA . Interestingly, a 20-fold increase in RPA binding to DNA was found when in complexed to mutant Rad52. The mutant Rad52 has no DNA binding capability which suggest that the Rad52 interaction with RPA is involved in regulating RPA single-strand DNA binding.

References

1) M. S. Park, Ludwig D. L., Stigger E., Lee S., *J. Biol. Chem., 271(31), 18996 (1996)*
2) S. Hays, Firminich A., Massay P., Banerjee R., Berg P., *Mol. Cell. Biol.*, 18(7),4400 (1998)
3) New J., Tomohiko S., Zaitseva E., Kowalczykowski S., *Nature,* 391, 407 (1998)
4) Mer g., A bocharev, R. Gupta, A. Edwards, W. Chazin, *Cell,* 103, 449 (2000)
5) Ranatunga W., D. Jackson, Lloyd J., Forget A., Knight K., Borgstahl G., *J. Biol. Chem., (published on Feb. 13, 2001)*

Wasantha Ranatunga, Human RAD52 has extreme thermal stability, The 22nd annual graduate research symposium, Sigma Xi scientific research society of the University of Toledo (April 20, 2001)

Human Rad52 protein has extreme thermal stability

Wasantha Ranatunga
Research Advisor: Dr. Gloria Borgstahl
Department of Chemistry
Phone: (419) 530 1581
Email: wranatunga@hotmail.com

Human Rad52 (hRAD52) is double-strand break repair protein involved in the homologous recombination pathway (1). The monomers of hRAD52 self-associate into rings as well as higher order aggregates of rings (2). hRAD52 binds to DNA double-strand ends and mediates strand exchange or end joining by higher order association (3). The thermal stability of hRAD52 was investigated using differential scanning calorimetry. In the profile of calorimetry, three transitions were observed at temperatures of 38.8, 73.1 and 115.2 °C. The two-domain mutant, hRAD52 (1-192) showed two transitions at 47.6 and 100.9 °C and does not form higher order aggregates of rings. Dynamic light scattering (DLS) was used to study structural changes of hRAD52 due to concentration and temperature. Data indicate an increase in aggregation with concentration. The aggregates of rings can be disrupted at higher temperatures. Aggregation of rings, as well as ring formation, appear to stabilize the fold and a four state hypothetical model was proposed to explain the thermal denaturation profile of wild-type hRAD52.

1. Shinohara, A., Shinohara, M., Ohta, T., Matsuda, S., and Ogawa, T. *Genes to Cells* **3**, 145, (1998).
2. Van Dyck, E., Hajibagheri, N. M. A., Stasiak, A., and West, S. C. *J. Mol. Biol.* **284**, 1027, (1998).
3. Van Dyck, E., Stasiak, A., and West, S. C. *Nature* **398**, 728, (1999).

Human RAD52 Protein Has Extreme Thermal Stability

Wasantha Ranatunga, Doba Jackson, Robert A. Flowers II, and Gloria E. O. Borgstahl

Department of Chemistry, The University of Toledo,
Toledo, Ohio 43606-3390

Biochemistry®

Human RAD52 Protein Has Extreme Thermal Stability[†]

Wasantha Ranatunga, Doba Jackson, Robert A. Flowers II, and Gloria E. O. Borgstahl*

Department of Chemistry, The University of Toledo, Toledo, Ohio 43606-3390

Received February 2, 2001; Revised Manuscript Received April 27, 2001

ABSTRACT: The human RAD52 protein plays an important role in the earliest stages of chromosomal double-strand break repair via the homologous recombination pathway. Individual subunits of RAD52 associate into seven-membered rings. These rings can form higher order complexes. RAD52 binds to DNA breaks, and recent studies suggest that the higher order self-association of the rings promotes DNA end joining. Monomers of the RAD52(1−192) deletion mutant also associate into ring structures but do not form higher order complexes. The thermal stability of wild-type and mutant RAD52 was studied by differential scanning calorimetry. Three thermal transitions (labeled A, B, and C) were observed with melting temperatures of 38.8, 73.1, and 115.2 °C. The RAD52(1−192) mutant had only two thermal transitions at 47.6 and 100.9 °C (labeled B and C). Transitions were labeled such that transition C corresponds to complete unfolding of the protein. The effect of temperature and protein concentration on RAD52 self-association was analyzed by dynamic light scattering. From these data a four-state hypothetical model was developed to explain the thermal denaturation profile of wild-type RAD52. The three thermal transitions in this model were assigned as follows. Transition A was attributed to the disruption of higher order assemblies of RAD52 rings, transition B to the disruption of rings to individual subunits, and transition C to complete unfolding. The ring-shaped quaternary structure of RAD52 and the formation of higher ordered complexes of rings appear to contribute to the extreme stability of RAD52. Higher ordered complexes of rings are stable at physiological temperatures in vitro.

RAD52[1] protein plays a critical role in mitotic and meiotic recombination as well as double-strand break repair (*1, 2*). On the basis of a series of protein−protein interaction assays and DNA binding studies (*3−5*), a domain map of human RAD52 (RAD52) was proposed by Park et al. (Figure 1). Electron microscopy (EM) studies of *Saccharomyces cerevisiae* and human RAD52 have revealed formation of ring-shaped structures (9−13 nm in diameter), as well as higher order aggregates (*6−8*). The RAD52 rings appear to be composed of seven subunits (*9*). EM studies also showed that RAD52 recognizes and binds to double-stranded DNA ends as an aggregated complex that ranges in size from approximately 15 to 60 nm in diameter (*8*). This binding promoted end-to-end association between DNA molecules and stimulated the ligation of both cohesive and blunt DNA ends (*8*). Recently, by studying wild type and two deletion mutants of RAD52 (Figure 1), we demonstrated that the self-association domain in the N-terminal half of RAD52 is responsible for ring formation and that elements in the C-terminal half of the molecule participate in the formation of higher order complexes of rings (*10*).

Due to the biological interest of human RAD52 and the apparent biochemical importance of RAD52 self-association in DNA repair, we studied its multiple levels of self-association and stability using biophysical methods. The stability of wild-type RAD52 was studied by differential scanning calorimetry (DSC). To investigate the basis for the extreme stability of RAD52 that was discovered, two mutants were also studied, RAD52(1−192) and RAD52(218−418) (Figure 1). The effects of temperature and protein concentration on the hydrodynamic radius (R_H) of RAD52 were studied by dynamic light scattering (DLS). Finally, a hypothetical model of the effects of protein aggregation state on thermal stability was developed.

MATERIALS AND METHODS

Protein Purification. The domain structures for wild-type RAD52, RAD52(1−192), and RAD52(218−418) are described in Figure 1. Proteins were expressed, purified under reducing conditions, and concentrated as described (*10*). Unfortunately, enterokinase cleavage was nonspecific, and the histidine-patch thioredoxin (Invitrogen) could not be separated from the 218−418 peptide (Jackson, unpublished results). After the extreme thermal stability of wild-type RAD52 was observed, subsequent purifications included a heat treatment step. The lysate was heated to 55 °C for 30 min prior to the chromatography steps. Samples were concentrated using an Ultrafree-15 centrifugal filter device. After each step of concentration, the samples were analyzed by DLS. Protein concentrations were determined using the Bradford assay (Bio-Rad) with bovine serum albumin as a standard.

¹ Abbreviations: RAD52, human RAD52; DLS, dynamic light scattering; DSC, differential scanning calorimetry; EM, electron microscopy; MnSOD, manganese superoxide dismutase; SOS, sum of squares; R_H, hydrodynamic radius; T_M, melting temperature.

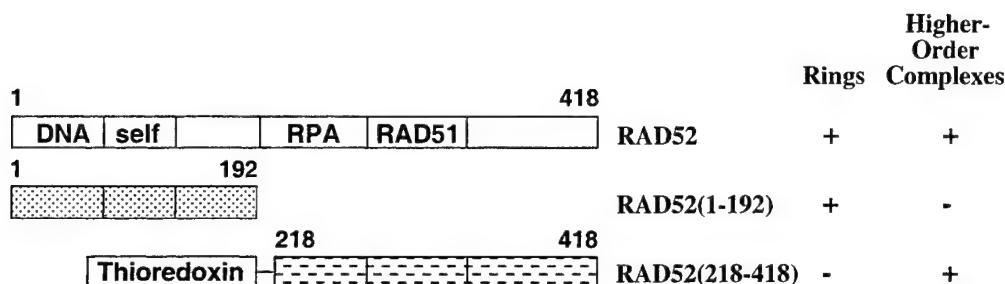|		Rings	Higher-Order Complexes
1 ... 418 DNA | self | | RPA | RAD51 |	RAD52	+	+
1 ... 192	RAD52(1-192)	+	-
218 ... 418 Thioredoxin |	RAD52(218-418)	-	+

FIGURE 1: Wild-type RAD52 and deletion mutants. Beginning and ending residue numbers of each mutant are indicated along with domain structure. The following domains and residue numbers were defined by Park et al. (*16*): DNA binding (39−80), self-association (85−159), RPA binding (221−280), and RAD51 binding (290−330). The structural characterization of wild-type and mutant RAD52 by Ranatunga et al. is summarized on the right (*10*). Wild-type RAD52 and RAD51(1−192) have six histidines fused to the C-terminus. For the RAD52-(218−418) mutant, a thrombin-cleavable six-histidine tag is fused to the N-terminus of the histidine-patch thioredoxin, and an enterokinase cleavage site separates histidine-patch thioredoxin from RAD52(218−418).

Differential Scanning Calorimetry. Protein and reference solutions were degassed under a vacuum for 15 min before data acquisition. The concentration of wild-type RAD52 was 2.0 and 3.5 mg/mL, RAD52(1−192) was 7.2 mg/mL, and RAD52(218−418) was 3.1 mg/mL. The wild-type RAD52 sample was concentrated to 11.5 mg/mL before dilution to either 2.0 or 3.5 mg/mL. The concentrations of wild-type RAD52 and RAD52(218−418) were limited by the quantity of protein available. The protein samples and reference solutions were loaded into their respective cells in the MicroCal MC-2 differential scanning calorimeter. An external pressure of 30 psi was applied with nitrogen gas to both sample and reference cells. The sample was scanned relative to the reference solution over a temperature range of 5−120 °C at a rate of 45 °C/h. DSC measurements on buffer alone had no transitions for the temperature range 5−120 °C. The baseline and change in specific heat (ΔC_p) upon denaturation were corrected according to standard techniques (*11*). DSC data were fit to a two- or three-state model using the Origin DSC software provided by Microcal Inc.

Dynamic Light Scattering Analysis. DLS was carried out using a DynaPro-801 molecular sizing instrument equipped with a temperature-controlled microsampler (Protein Solutions). A 50 μL sample was passed through a filtering assembly equipped with a 100 nm filter into a 12 μL chamber quartz cuvette. For each experiment, 35−60 measurements were taken. The data were first analyzed using Dynamics 4.0 software and then with DynaLS software. The refractive index and viscosity of the buffer at each temperature were measured and the proper corrections applied to the data. Baseline and sum of squares (SOS) error values were reported by Dynamics 4.0. The baseline is the measured value of the last coefficient in the correlation curve. Baselines within the range from 0.977 to 1.002 were interpreted as monomodal, and those greater than 1.002 were bi- or multimodal. The SOS error is the sum of squares difference between the measured correlation curve and the best-fit curve. SOS errors less than 5.000 were considered negligible. Errors between 5.000 and 20.000 were considered as low and probably due to low protein concentration or a small amount of polydispersity. Errors greater than 20.000 were considered as high and are probably due to high polydispersity in size distribution (aggregation) or irregular solvent. Mean R_H, standard deviation, and percent of peak area are reported from DynaLS using the optimized resolution. Due to the irregular solvent, the SOS errors increased for diluted samples, and it was necessary to use DynaLS to separate the solvent peak from the protein peak.

RESULTS AND DISCUSSION

Differential Scanning Calorimetry. Thermal stability profiles of wild-type RAD52, RAD52(1−192), and RAD52-(218−418) were obtained by DSC (Figure 2 and Table 1). For wild-type RAD52 and RAD52(1−192) the DSC transitions were labeled A, B, or C such that total unfolding was always labeled C. For wild-type RAD52, at 2.0 mg/mL, the DSC profile was composed of two transitions (labeled B and C) with melting temperatures (T_M) of 78.3 and 101.6 °C (Table 1). At 3.5 mg/mL, the wild-type RAD52 DSC profile was composed of three distinct transitions (labeled A, B, and C in Figure 2A) with T_M's of 38.8, 73.1, and 115.2 °C (Table 1). When the concentration of wild-type RAD52 was increased, transition C was shifted to a higher temperature by 13 °C. Transition A could be measured only if the sample was first concentrated to 11.5 mg/mL and then diluted to 3.5 mg/mL. For RAD52(1−192) two transitions were observed at 47.6 and 100.9 °C (labeled B and C in Figure 2B). The deletion of the C-terminal half of RAD52 decreased the T_M of transitions B and C by 25 and 14 °C, respectively.

Our earlier analysis demonstrated that wild-type RAD52 forms ring structures as well as higher order complexes of rings but RAD52(1−192) forms rings but not the aggregates of rings (*10*). The size of the wild-type RAD52 higher order complexes, as well as the proportion of the rings in a higher order complex, is dependent on concentration. RAD52(1−192) rings do not form higher ordered complexes, at any concentration. DSC transition A was dependent on the concentration of wild-type RAD52 and was not observed for RAD52(1−192). Therefore, it appeared that transition A corresponded to the thermal disruption of aggregates to form single rings in solution, transition B to the break up of rings to monomers, and transition C to the total unfolding of monomers.

The DSC profile of RAD52(218−418) is also consistent with this interpretation (Figure 2C). RAD52(218−418) forms a complex of two to four monomers depending on the concentration but does not form ring structures in solution (*10*). It has a relatively low T_M of 53−59 °C, and it appears that the C-terminal half of RAD52, which cannot form rings, is not as thermally stable as the ring-structured N-terminal half.

Wild-type *Escherichia coli* thioredoxin is a very stable protein with a T_M of ∼85 °C for the oxidized form and ∼73
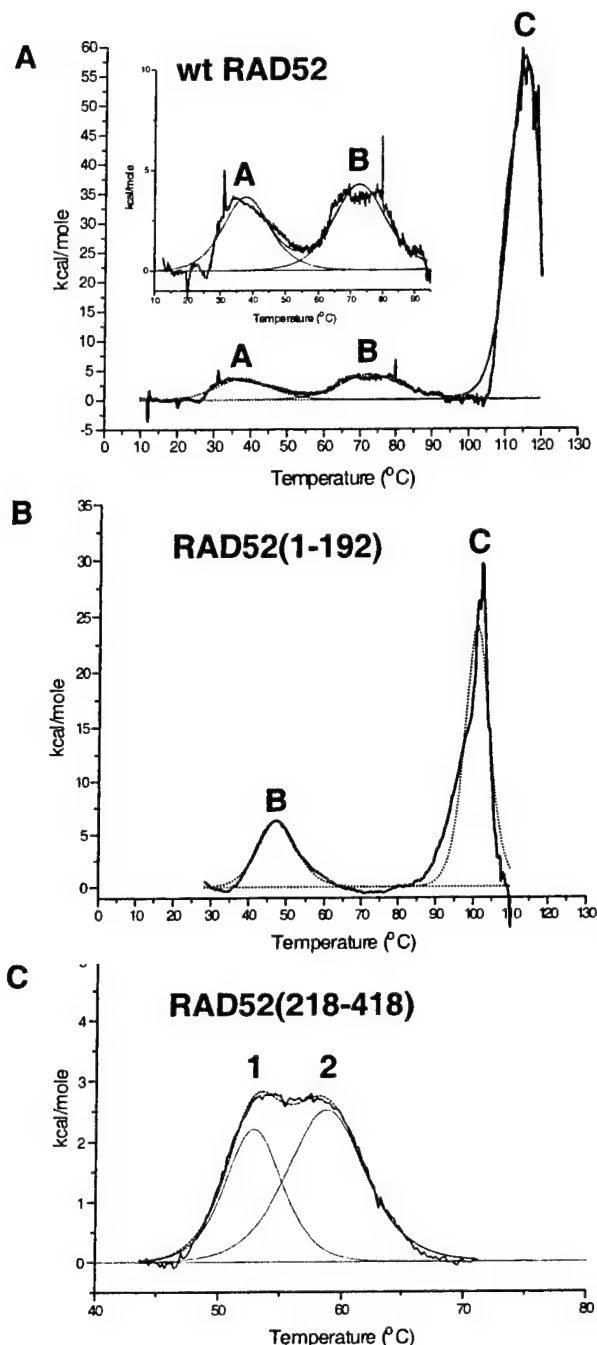
FIGURE 2: Thermal stability of wild-type RAD52 and deletion mutants. DSC profiles for (A) wild-type RAD52 were analyzed at 0.038 mM (3.5 mg/mL), (B) RAD52(1−192) at 0.325 mM (7.2 mg/mL), and (C) RAD52(218−418) at 0.082 mM (3.1 mg/mL). For RAD52(218−418) there were no transitions above 70 °C.

Table 1: Thermodynamic Parameters from DSC Measurement of RAD52 Proteins

protein	concn (mg/mL)	component	T_M (°C)
RAD52[a]	2.0	B	78.3
		C	101.6
RAD52[b]	3.5	A	38.8
		B	73.1
		C	115.2
RAD52(1−192)[c]	7.2	B	47.6
		C	100.9
RAD52(218−418)[d]	3.1	1	53.4
		2	59.1

[a] This sample was concentrated to 11.5 mg/mL and then diluted to 2.0 mg/mL (similar to Table 2, line 12) and does not contain higher ordered assemblies of rings. [b] This sample was concentrated to 11.5 mg/mL and then diluted to 3.5 mg/mL for DSC measurements (similar to Table 2, line 7, and Figure 3E) and contains higher ordered complexes of rings. [c] RAD52(1−192) forms rings but does not form higher ordered assemblies of rings (10). [d] RAD52(218−418) does not form rings but does self-associate (10).

°C for the reduced form (12, 13). When thioredoxin is fused to other proteins, it can improve their solubility and, especially when in the oxidized form, improve their thermal stability, allowing a heat step during purification. Histidine-patch thioredoxin in the reduced state was expected to have a T_M of ∼67 °C (12−14). We were unable to specifically cleave thioredoxin from RAD52(218−418) with enterokinase, so the exact contributions of thioredoxin and RAD52-(218−418) to the DSC profile of the fusion protein could not be determined. It is apparent that fusing thioredoxin to RAD52(218−418) has reduced the T_M of thioredoxin significantly and that RAD52(218−418) by itself would prob-

ably have a T_M lower than that measured for the fusion protein.

The reversibility of transitions A, B, and C for wild-type RAD52 was studied by DSC, using an 11.5 mg/mL sample diluted to 3.5 mg/mL. Three experiments were performed, and the presence of precipitation was noted after each (data not shown). First, the sample was heated to 55 °C and then slowly returned to 20 °C overnight. Transition A was observed, and the protein remained in solution. Then the same sample was heated to 95 °C and slowly returned to 20 °C overnight. During this second experiment, transition A did not return, possibly due to the protein concentration used (see discussion of DLS data, Table 2, lines 7−9), and transition B was lowered to 65 °C. After the second experiment there was a slight amount of precipitate, but the majority of the protein was still in solution. For the third experiment, the sample was heated to 120 °C, and there was only one significant peak at 94 °C and the protein completely precipitated. The T_M for complete unfolding was lower than that measured from fresh sample (115 °C for peak C, Figure 2A), indicating that the protein did not properly reassemble after the second experiment and that the process of unfolding is irreversible under this set of experimental conditions.

The irreversibility of transition B was also noted in experiments performed during the addition of a heat step to the purification protocol for wild-type RAD52. Lysates were heated in 5 deg increments between 55 and 80 °C, centrifuged, and analyzed by SDS−PAGE. RAD52 began to precipitate after 65 °C (data not shown). This supports the conclusion that transition B in the thermal denaturation of RAD52 is irreversible.

Dynamic Light Scattering. The response of RAD52 rings and higher ordered complexes to concentration and temperature was studied by DLS. The upper temperature limit of the DLS microsampler was 50 °C so theoretically data on transition A of wild-type RAD52 and transition B of RAD52-(1−192) could be measured.

The procedure followed for sample preparation affected the detection of DSC transition A and the T_M value of transition C for wild-type RAD52, so the effects of protein concentration and temperature on the R_H of wild-type RAD52 were studied using DLS. In a series of experiments, the protein concentration was increased from 3.5 to 11.5 mg/

Table 2: Effect of Temperature and Concentration on R_H of Wild-Type RAD52

DLS expt	concn (mg/mL)	base-line	SOS error[a]	R_H[b] (nm)	peak area[c] (%)	interpre-tation[d]
1. 20 °C	3.5	1.001	4.22	**15.0 (2.5)**	**98.3**	>2 rings
2. heat to 50 °C	3.5	1.000	2.78	**14.2 (4.5)**	**99.2**	~2 rings
3. concd; 20 °C	4.9	1.002	2.03	4.3 (0.5)	3.4	monomer
				18.7 (2.3)	**95.8**	>2 rings
4. concd; 20 °C	11.5	1.009	7.78	5.1 (0.6)	4.2	mono/dimer
				17.8 (3.1)	**56.9**	>2 rings
				36.1 (4.4)	**36.6**	≫2 rings
5. heat to 50 °C	11.5	1.000	5.96	**19.2 (8.5)**	**99.2**	>2 rings
6. cool to 20 °C	11.5	1.010	8.24	5.9 (0.4)	9.7	mono/dimer
				11.2 (0.7)	6.6	1–2 rings
				20.6 (2.2)	**81.6**	>2 rings
7. sample from line 4 diluted; 20 °C	3.5	1.001	11.3	3.8 (0.2)	0.6	monomer
				23.2 (11.6)	**98.1**	>2 rings
8. heat to 50 °C	3.5	1.001	9.41	**9.7 (1.2)**	**45.8**	1 ring
				17.0 (1.0)	**49.8**	>2 rings
9. cool to 20 °C	3.5	1.001	16.1	3.9 (0.2)	1.1	monomer
				11.9 (1.9)	**69.3**	1–2 rings
				28.6 (3.5)	**26.4**	≫2 rings
10. sample from line 3 diluted; 20 °C	3.3	1.001	7.4	**3.1 (0.2)**	**11.0**	monomer
				16.8 (5.4)	**84.0**	>2 rings
				49.5 (8.7)	**14.5**	≫2 rings
11. heat to 37 °C	3.3	1.000	7.9	**19.8 (10.9)**	**99.5**	>2 rings
12. sample from line 4 diluted; 20 °C	2.3	1.001	50.9	**8.75 (6.0)**	**79.7**	1 ring
13. heat to 37 °C	2.3	1.000	24.5	**8.0 (1.6)**	**71.9**	1 ring
14. heat to 50 °C	2.3	1.000	15.9	**8.7 (2.7)**	**87.4**	1 ring

[a] SOS = sum of squares. [b] Average R_H is given with the standard deviation given in parentheses. [c] DynaLS results; the percent peak area for the solvent peaks was not reported. DLS measurements at 20 and 50 °C on solvent alone indicate that very small and very large components in the RAD52 measurements were due to the solvent and not the protein. Therefore, only the peaks attributable to RAD52 protein are reported ($R_H > 3.0$ nm; see Figure 4). R_H and percent peak area of the primary species in solution (greater than 10%) are in bold. [d] Interpretation is based on estimated R_H in Figure 4. It is not possible to tell exactly how many rings of RAD52 are in the aggregates >14.1 nm since the structure of the higher order complexes of RAD52 rings is unknown.

mL and then diluted (see Table 2 and Figure 3). The microsampler cell was held at 20, 37, or 50 °C, and samples were equilibrated for 30 min at the target temperature before DLS measurements began. The smallest R_H measured for RAD52 was 8.0–8.75 nm (Table 2, lines 12–14). This is close to the size expected for single rings measured from electron micrographs (Figure 4) (*6–8*). A monomer of RAD52 is expected to have an R_H value of 3.2 nm, and complexes containing two rings are expected to have an R_H of 12.8–14.1 nm. The R_H for aggregates of more than two rings would be greater than 14 nm.

Using these estimates of particle sizes as a guide, four trends in the DLS data were noted. First, heating the protein samples from 20 to 50 °C caused the R_H to decrease in general, and frequently the baseline decreased to within the monomodal range. For example, heating a sample similar to that used for DSC measurements (Table 2, line 7, and Figure 3E) caused the particles to shift from a single population with R_H of 23.2 nm to two populations with R_H of 9.7 and 17.0 nm (Table 2, line 8, and Figure 3F). Second, the size of the sample population was dependent on the protein concentration. For example, the R_H of the sample
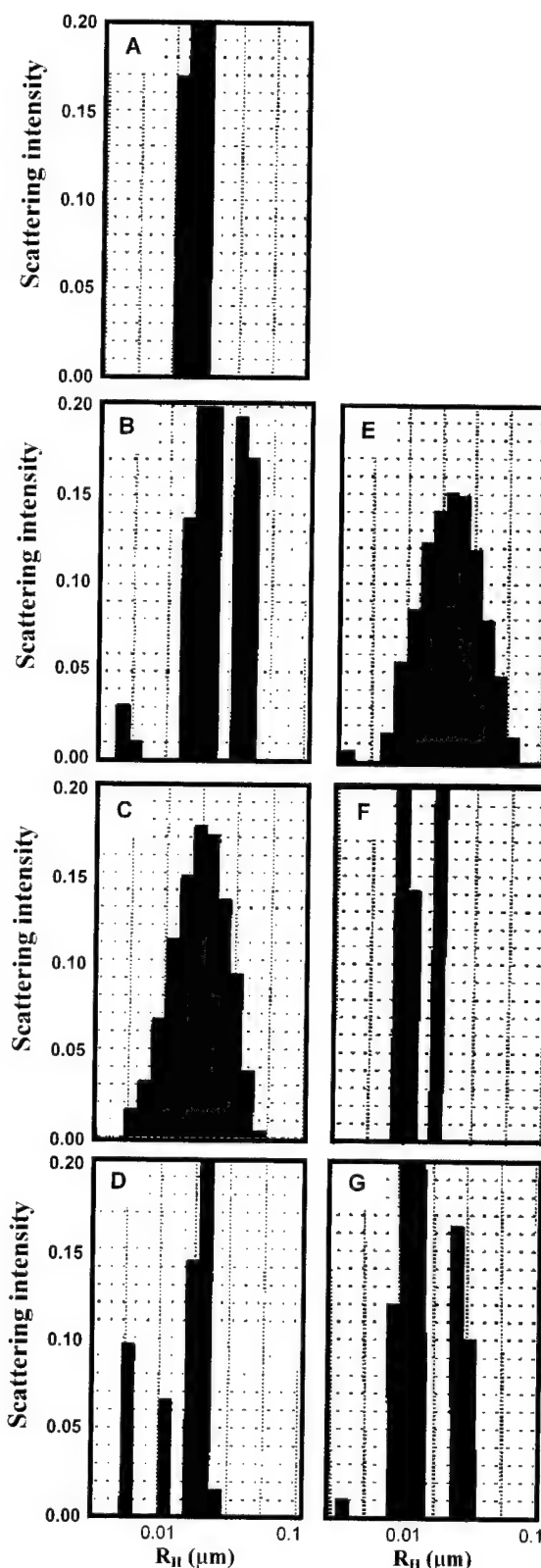

FIGURE 3: Effect of protein concentration and temperature on the R_H of wild-type RAD52. DLS data were analyzed using DynaLS software. The data correspond to the following lines in Table 2: (A) 3.5 mg/mL at 20 °C (line 1), (B) 11.5 mg/mL at 20 °C (line 4), (C) 11.5 mg/mL at 50 °C (line 5), (D) 11.5 mg/mL cooled to 20 °C (line 6), (E) diluted to 3.5 mg/mL at 20 °C (line 7), (F) diluted to 3.5 mg/mL at 50 °C (line 8), and (G) diluted to 3.5 mg/mL cooled to 20 °C (line 9). Panels E–G correspond to the sample used for DSC.

Model	R_H (nm)
Monomer	3.2
7-membered ring	8.5
Two edge on rings	14.1
Two stacked rings	12.8

FIGURE 4: Estimated R_H for RAD52 models. The R_H for a monomer was calculated from a molecular mass of 47.0 kDa with the molecular weight calculator included in the Dynamics 3.0 software. R_H for a seven-membered ring of RAD52 was estimated from the diagonal of the three-dimensional reconstruction on the basis of electron micrographs (9). Electron micrographs of RAD52 rings in the large, greater than 100 nm spherical aggregates appear to have an "edge-on" orientation (10). The three-dimensional reconstructions of RAD52 were adapted from Stasiak et al. (2000).

population increased from 15.0 to 18.7 to 36.1 nm, when the concentration was increased from 3.5 to 4.9 to 11.5 mg/mL (Table 2, lines 1, 3, and 4). Third, the modality of the sample population was dependent on the protein concentration. For example, the 11.5 mg/mL sample was multimodal at 20 °C (Table 2, line 4, and Figure 3B), and the 3.5 mg/mL sample was not (Table 2, line 1, and Figure 3A). Fourth, the reversibility of the assembly of RAD52 rings into higher ordered complexes was dependent on protein concentration. The majority of the particles in the samples at 11.5 mg/mL remained greater than 17 nm throughout the heat cycle (Table 2, lines 4–6, and Figure 3B–D). But, the superaggregation of rings was only partially reversible at 3.5 mg/mL with only 26% of the sample returning to greater than 17 nm after being heated (Table 2, lines 7–9, and Figure 3E–G). It is noteworthy that for the DSC measurements made on samples at 3.5 mg/mL the assembly of RAD52 rings into higher ordered complexes is not completely reversible at this concentration.

Finally, this DLS analysis facilitated the interpretation of DSC transition A. Transition A could not be detected for samples that were first concentrated to 11.5 mg/mL and then diluted to 2.0 mg/mL (prepared as in line 12, Table 2). The R_H value of 8.75 indicates that at 2.0 mg/mL there are primarily single rings in solution and little or no higher ordered complexes (Figure 4). Transition A was detectable for samples that were diluted to 3.5 mg/mL (prepared as in line 7, Table 2, and Figure 3E). The R_H value of 23.2 nm indicates that at 3.5 mg/mL there are primarily higher order complexes of many rings in solution. Heating this sample to 50 °C caused the R_H to decrease and form two populations of 9.7–17.0 nm (Table 2, line 8, and Figure 3F). Therefore, these DLS data indicate that DSC transition A can be attributed to the disassociation of rings from higher ordered complexes.

We were interested to know if the higher ordered complexes of RAD52 rings were stable at physiological temperatures. Protein samples diluted to 3.3 mg/mL did not form particles less than 9 nm upon heating to 37 °C (Table 2, lines 10 and 11) although the samples became monomodal. Therefore, the upper level aggregation of RAD52 rings is stable at physiological temperatures in vitro.

Transition B of the RAD52(1−192) mutant was 47.6 °C, and attempts were made to measure the effect of temperature on the structure of RAD52(1−192) with DLS. Higher ordered assemblies of rings are not formed by RAD52(1−
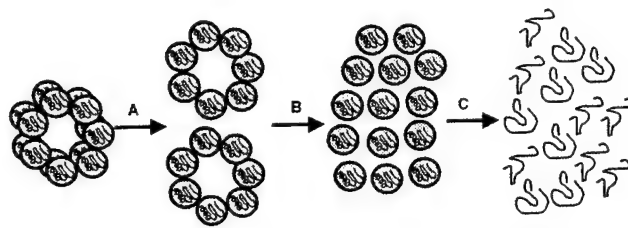

FIGURE 5: Hypothetical four-state model for the thermal denaturation of wild-type RAD52. Transitions A, B, and C correspond to those measured by DSC in Figure 2. There are three transitions in this model; transition A is attributed to the disruption of higher order assemblies of RAD52 rings, transition B to the disruption of rings to individual subunits, and transition C to complete unfolding. The individual subunits after transition B are probably partially unfolded as well as disassociated from the rings.

192), and single rings have an R_H of 5.7 nm (SD = 1.2) (10). As samples of RAD52(1−192) were heated, the R_H appeared to increase, perhaps indicating partial unfolding (data not shown). DLS measurements at elevated temperatures with RAD52(1−192) were very problematic, and at 50 °C no measurements could be obtained, perhaps due to large changes in structure.

CONCLUSIONS

Our data indicate that the RAD52 rings and higher ordered complexes of rings used in DNA repair and DNA recombination are extremely stable structures. The structure of wild-type RAD52 is very stable, and its multiple levels of self-association appear to contribute to this stabilization. The extreme stability of the wild-type RAD52 and RAD52(1−192) folds relative to RAD52(218−418) appears to be related to the assembly of multiple monomers into a ring. The enhanced stability of the wild-type RAD52 fold relative to RAD52(1−192) appears to be due in part to its ability to form higher order assemblies of rings.

A four-state hypothetical model has been developed to explain the thermal denaturation profile of wild-type RAD52 (Figure 5). There are three transitions in this model; transition A is attributed to the disruption of higher order assemblies of RAD52 rings, transition B to the disruption of rings to individual subunits, and transition C to complete unfolding. Individual rings of RAD52 appear to have an R_H on the order of 8.0–8.75 nm in solution (Table 2, lines 12−14). Higher order assemblies of rings are seen in the wild-type RAD52 DLS data as particles ranging from 15 to 50 nm. Note that the measured R_H values are not integral values of individual rings due to the presence of equilibrium mixtures of single rings and complexes of rings in solution as indicated by the high standard deviations in the R_H measurements (Table 2) and the width of the DLS peaks (Figure 3). This equilibrium is dependent upon concentration. At concentrations of 3.5 mg/mL or greater RAD52 appears to be primarily composed of assemblies of two or more rings with R_H values ranging from 15 to 36.1 nm. Raising the temperature from 20 to 50 °C disrupts the higher order particles, pushing the equilibrium toward the 9 nm particles (Table 2, lines 5 and 8, and Figure 3C and F). These data support our hypothetical model for transition A (Figure 5). Reliable DLS measurements varying temperature on RAD52(1−192) could not be made. Thermal expansion of the RAD52(1−192) rings was noted. The data indicate that a large structural transition occurs near transition

B, possibly the disassociation of individual subunits from the rings.

Only a handful of proteins have been measured with thermal stabilities on the order of RAD52. To our knowledge, the highest T_M for a protein reported in the literature to date is 125 °C for ferredoxin from the hyperthermophile *Thermotoga maritima* (*15*). Other proteins such as onconase and mitochondrial manganese superoxide dismutase (MnSOD) are extremely stable with T_M's approaching 90 °C (*16, 17*). Both ferredoxin and onconase are monomeric, and by studying their protein crystal structures, their stabilities were attributed to the compactness of their tertiary structures and to extensive hydrogen bonding involving charged amino acid side chains. Mitochondrial MnSOD is a homotetramer, and its enhanced stability was partially attributed to its quaternary structure. The DSC profile of MnSOD has three thermal transitions (labeled A, B, and C), similar to those seen with RAD52. Transition A was attributed to subunit disassociation, transition B to loss of the active site manganese, and transition C to complete unfolding. A cavity forming point mutation in the tetrameric interface of MnSOD resulted in the lowering of transition B by 13.6 °C and transition C by 16.5 °C (*17*). These results on MnSOD are somewhat similar to the results on RAD52. We conclude from our data that both components of RAD52 self-association, ring formation and higher order complex formation, contribute to its extreme thermal stability. A precise understanding of the structural determinants of RAD52 stability awaits the solution of its crystal structure.

ACKNOWLEDGMENT

REFERENCES

1. Game, J., and Mortimer, R. K. (1974) *Mutat. Res. 24*, 281−292.

2. Petes, T. D., Malone, R. E., and Symington, L. S. (1991) in *The Molecular and Cellular Biology of the Yeast, Saccharomyces* (Broach, J. R., Pringle, J. R., and Jones, E. W., Eds.) pp 407−522, Cold Spring Harbor Laboratory Press, Cold Spring Harbor, NY.

3. Shen, Z., Cloud, K. G., Chen, D. J., and Park, M. S. (1996) *J. Biol. Chem. 271*, 148−152.

4. Shen, Z., Peterson, S. R., Comeaux, J. C., Zastrow, D., Moyzis, R. K., Bradbury, E. M., and Chen, D. J. (1996) *Mutat. Res. 364*, 81−89.

5. Park, M. S., Ludwig, D. L., Stigger, E., and Lee, S. H. (1996) *J. Biol. Chem. 271*, 18996−19000.

6. Shinohara, A., Shinohara, M., Ohta, T., Matsuda, S., and Ogawa, T. (1998) *Genes Cells 3*, 145−156.

7. Van Dyck, E., Hajibagheri, N. M. A., Stasiak, A., and West, S. C. (1998) *J. Mol. Biol. 284*, 1027−1038.

8. Van Dyck, E., Stasiak, A. Z., Stasiak, A., and West, S. C. (1999) *Nature 398*, 728−731.

9. Stasiak, A. Z., Larquet, E., Stasiak, A., Muller, S., Engel, A., Dyck, E. V., West, S. C., and Egelman, E. H. (2000) *Curr. Biol. 10*, 337−340.

10. Ranatunga, W., Jackson, D., Lloyd, J. A., Forget, A. L., Knight, K. L., and Borgstahl, G. E. O. (2001) *J. Biol. Chem.* (in press).

11. Haynie, D. T., and Freire, E. (1994) *Anal. Biochem. 216*, 33−41.

12. Ladbury, J., Wynn, R., Hellinga, H., and Sturtevant, J. (1993) *Biochemistry 32*, 7526−7530.

13. Ladbury, J., Kishore, N., Hellinga, H., Wynn, R., and Sturtevant, J. (1994) *Biochemistry 33*, 3688−3692.

14. Lu, Z., DiBlasio-Smith, E., Grant, K., Warne, N., LaVallie, E., Collins-Racie, L., Follettie, M., Williamson, M., and McCoy, J. (1996) *J. Biol. Chem. 271*, 5059−5065.

15. Pfeil, W., Gesierich, U., Kleemann, G. R., and Sterner, R. (1997) *J. Mol. Biol. 272*, 591−596.

16. Notomista, E., Catanzano, F., Graziano, G., Piaz, F. D., Barone, G., D'Alessio, G., and Donato, A. D. (2000) *Biochemistry 39*, 8711−8718.

17. Borgstahl, G. E. O., Parge, H. E., Hickey, M. J., Johnson, M. J., Boissinot, M., Hallewell, R. A., Lepock, J. R., Cabelli, D. E., and Tainer, J. A. (1996) *Biochemistry 35*, 4287−4297.

Human RAD52 Exhibits Two Modes of Self-association*

Wasantha Ranatunga‡§, Doba Jackson‡§, Janice A. Lloyd§¶, Anthony L. Forget§¶, Kendall L. Knight¶, and Gloria E. O. Borgstahl‡‖

From the ‡Department of Chemistry, University of Toledo, Toledo, Ohio 43606-3390 and the ¶Department of Biochemistry and Molecular Pharmacology, University of Massachusetts Medical School, Worcester, Massachusetts 01655-0103

The human RAD52 protein plays an important role in the earliest stages of chromosomal double-strand break repair via the homologous recombination pathway. Individual subunits of RAD52 self-associate into rings that can then form higher order complexes. RAD52 binds to double-strand DNA ends, and recent studies suggest that the higher order self-association of the rings promotes DNA end-joining. Earlier studies defined the self-association domain of RAD52 to a unique region in the N-terminal half of the protein. Here we show that there are in fact two experimentally separable self-association domains in RAD52. The N-terminal self-association domain mediates the assembly of monomers into rings, and the previously unidentified domain in the C-terminal half of the protein mediates higher order self-association of the rings.

The repair of double-strand breaks in chromosomal DNA is of critical importance for the maintenance of genomic integrity. In *Saccharomyces cerevisiae*, genes of the *RAD52* epistasis group, *RAD50*, *RAD51*, *RAD52*, *RAD54*, *RAD55*, *RAD57*, *RAD59*, *MRE11*, and *XRS2*, were identified initially by the sensitivity of mutants to ionizing radiation (1, 2). These genes have been implicated in an array of recombination events including mitotic and meiotic recombination as well as double-strand break repair. *RAD52* mutants show the most severe pleiotropic defects suggesting a critical role for the protein in homologous recombination and double-strand break repair (2). The importance of specific protein-protein interactions in the catalysis of homologous recombination is suggested by studies demonstrating specific contacts and functional interactions between Rad52p and a number of proteins involved in recombination including Rad51p (3–8), which catalyzes homologous pairing and strand exchange, and replication factor A (RPA)[1] (8–10), a heterotrimeric single-stranded DNA binding protein (11).

Studies of the equivalent human proteins have identified similar interactions between the RAD52, RAD51, and replication protein A proteins (12–17). Based on a series of protein-protein interaction assays (15, 16, 18) and DNA binding studies[2] (16), a domain map of RAD52 was proposed by Park *et al.* (16) (see Fig. 1). The determinants of self-association were proposed to exist exclusively within a region defined by residues 65–165, a result supported by recent studies of several isoforms of RAD52 (19). Electron microscopy (EM) studies of Rad52p and RAD52 have revealed formation of ring-shaped structures (9–13 nm in diameter), as well as higher order aggregates (9, 12, 20). Stasiak *et al.* (21) performed image analyses of negatively stained electron micrographs and determined that the 10-nm RAD52 rings are composed of seven subunits. Scanning transmission electron microscopy (STEM) analysis indicated a mean mass of 330 ± 59 kDa supporting a heptameric ring-shaped RAD52 structure (21). Recent studies show that RAD52 binds to double-stranded DNA ends as an aggregated complex (20). These end-binding complexes were amorphous in shape and ranged in size from 15 to 60 nm. Within these complexes, RAD52 rings were observed occasionally. Binding of RAD52 to the DNA ends promoted end-to-end association between DNA molecules and stimulated ligation of both cohesive and blunt DNA ends (20).

Therefore, given that the formation of both ring-shaped oligomers and aggregates of these rings seem relevant to RAD52 function, we sought to investigate further the self-association properties of the RAD52 protein. We performed a series of analyses comparing full-length RAD52-(1–418) with two different mutant RAD52 proteins: (i) a 1–192 mutant that spans the N-terminal portion and includes the entire proposed DNA binding and self-association domains and (ii) a 218–418 mutant that spans the C-terminal portion of RAD52 that includes the proposed RPA- and RAD51-binding domains (Fig. 1). In contrast to previous studies, our results show that there are experimentally separable determinants for two different modes of self-association by RAD52, one in the N-terminal and one in the C-terminal portion of the protein.
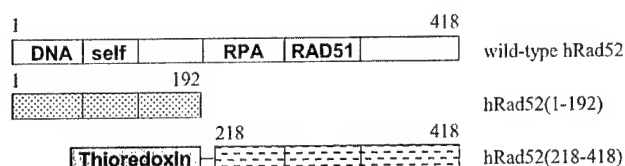
EXPERIMENTAL PROCEDURES

RAD52 Constructs—Wild-type *RAD52* and *RAD52*-(1–192) pET28 expression plasmids were a gift from Dr. M. Park and have six histidines fused to the C terminus. A pET28 expression plasmid containing the thioredoxin-RAD52-(218–418) fusion protein was constructed using standard polymerase chain reaction techniques.

Protein Purification—Cultures of transformed BL21(DE3) Codon Plus *Escherichia coli* (Stratagene) were grown in a fermentor and induced with 0.5 mM isopropyl-1-thio-β-D-galactopyranoside. Wild-type *RAD52* and *RAD52*-(1–192) cells were resuspended in a buffer consisting of 20 mM HEPES, pH 6.0, 10% glycerol, 400 mM NaCl, 100 mM KCl, 5 mM β-mercaptoethanol, 1 mM dithiothreitol, 1 mM hexylglucopyranoside, and 1 mM EDTA. *RAD52*-(218–418) cells were resuspended in a

§ These authors contributed equally to this work.

‖ To whom correspondence should be addressed: Dept. of Chemistry, University of Toledo, 2801 W. Bancroft St., Toledo, OH 43606-3390. Tel.: 419-530-1501; Fax: 419-530-4033; E-mail: gborgst@uoft02.utoledo.edu.

[1] The abbreviations used are: RPA, replication protein A; MES, 4-morpholineethanesulfonic acid; EM, electron microscopy; STEM, scanning transmission electron microscopy; BSA, bovine serum albumin; DLS, dynamic light scattering.

[2] J. A. Lloyd, and K. L. Knight, unpublished data.

This paper is available on line at http://www.jbc.org

FIG. 1. **Schematic diagram of wild-type RAD52 and deletion mutants.** The beginning and ending residue numbers of each mutant are indicated along with domain structure. The following domains and residue numbers were defined by Park *et al.* (16): DNA binding, 39–80; self-association, 85–159; RPA binding, 221–280; RAD51 binding, 290–330.

buffer consisting of 50 mM HEPES, pH 8, 500 mM KCl, 500 mM LiSO₄, 2.5% glycerol, 1 mM EDTA, 5 mM dithiothreitol, 4 mM imidazole, and 0.1% Triton X-100. Protease inhibitors (1 mM phenylmethylsulfonyl fluoride and 10 mM benzamidine) were used throughout purification. Cells were lysed using a French press, and the lysate was clarified by centrifugation, filtration through Cell Debris Remover-modified cellulose (Whatman), and passage through a 0.22-μm pore filter. The clarified lysate was applied to an MC/M Ni²⁺ affinity column (PerSeptive Biosystems) that was optimally washed and eluted with an imidazole gradient. Wild-type RAD52 and RAD52-(1–192) then were dialyzed extensively against a buffer consisting of 20 mM MES, pH 6.0, 10% glycerol, 400 mM NaCl, 100 mM KCl, 5 mM β-mercaptoethanol, 1 mM dithiothreitol, 1 mM hexylglucopyranoside, and 1 mM EDTA. RAD52-(218–418) was dialyzed extensively against a buffer consisting of 50 mM HEPES, pH 8.0, 2.5% glycerol, 2.5 mM EDTA, and 0.5 mM hexylglucopyranoside and then purified further by anion exchange using an HQ/M column (PerSeptive Biosystems) eluted with a KCl gradient. Protein samples were concentrated using Amicon concentrators with YM10 membranes, and protein concentrations were determined using Bradford assay (Bio-Rad) with bovine serum albumin (BSA) as a standard. The expression plasmid for wild-type RPA heterotrimer was a gift from Dr. M. Wold. RPA was expressed and purified as described (22).

Enzyme-linked Immunosorbent Assay—The enzyme-linked immunosorbent assay was done at room temperature. Briefly, 10 pmol of wild-type RAD52, RAD52 mutants, or BSA were coated to microtiter plates for 1 h. Plates were washed three times with phosphate-buffered saline (PBS) containing 0.02% Tween 20 to remove unbound protein. Plates then were blocked with 5% milk in PBS for 10 min and then washed. Various amounts of RPA in PBS and 5% milk were added and incubated for 1 h. Plates then were washed to remove nonspecific interactions and probed with a monoclonal antibody against the 70-kDa subunit of RPA (Calbiochem) in PBS and 5% milk for 30 min. Plates then were washed and probed with anti-mouse IgG peroxidase conjugate (Sigma) in PBS and 5% milk for 30 min and washed. Plates were developed using 3,3′,5,5′-tetramethylbenzidine in phosphate-citrate buffer with 0.03% hydrogen peroxide. Color was developed for 30 min, the reaction was stopped with 1.5 M H₂SO₄, and absorbance readings at 450 nm were taken with a microtiter plate reader. Background absorbance was determined from a blank well and then subtracted from the data.

Gel-shift DNA Binding Assays—Reactions (20 μl) contained 20 mM triethanolamine-HCl, pH 7.5, 1 mM dithiothreitol, 1 mM MgCl₂, 0.1 mg/ml BSA, 0.05% Tween 20, 2 nM 5′-end-labeled 95 base oligonucleotide (concentration in bases), and the indicated amounts of protein. The oligonucleotide sequence is as follows: 5′-AGA CGA TAG CGA AGG CGT AGC AGA AAC TAA CGA AGA TTT TGG CGG TGG TCT GAA CGA CAT CTT TGA GGC GCA GAA AAT CGA GTG GCA CTA ATA AG-3′. Reactions were incubated at 37 °C for 20 min followed by the addition of glutaraldehyde to 0.2% and continued incubation at 22 °C for 20 min. Glycerol was added to a final concentration of 1.6% (w/v) and samples (10 μl) were loaded onto a 0.8% agarose gel and electrophoresed at 100 mV in 0.5× TBE buffer (90 mM Tris, 64.6 mM boric acid, and 2.5 mM EDTA, pH 8.3). Gels were analyzed using a Molecular Imager FX and QuantityOne software (Bio-Rad). The 95-base oligonucleotide used in the gel-shift assays was made using an ABI 392 DNA/RNA synthesizer.

Dynamic Light-scattering (DLS) Analysis—DLS was carried out using a DynaPro-801 molecular sizing instrument equipped with a microsampler (Protein Solutions). A 50-μl sample was passed through a filtering assembly into a 12-μl chamber quartz cuvette. For RAD52-(1–192) and RAD52-(218–418), 20-nm filters were used. For wild-type RAD52, a 100-nm filter was used. The data were analyzed first using Dynamics 4.0 software and then DynaLS software as follows. Hydrodynamic radii (R_H) for monomodal distributions, as defined by a baseline ranging from 0.977 to 1.002, were reported from Dynamics 4.0. Bi- and multimodal distributions were analyzed using DynaLS. DynaLS data estimates of molecular weight were obtained from R_H using Dy-
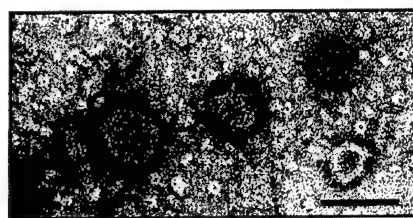
FIG. 2. **Negative stained electron micrograph of wild-type RAD52.** Wild-type RAD52 (4.0 μM) was prepared as described under "Experimental Procedures." Larger spherical particles are ~80 nm in diameter, half-spheres are 50 nm, and numerous 10-nm rings are visible also. *Black bar* = 0.1 μm.
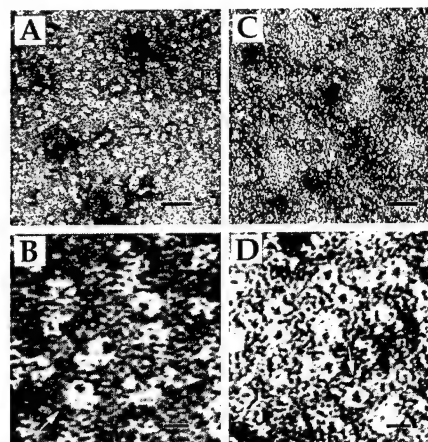
FIG. 3. **Negative stained electron micrographs of wild-type RAD52 and RAD52-(1–192) protein.** Proteins (4.0 μM) were prepared as described under "Experimental Procedures." The majority of protein for both wild-type RAD52 (*A* and *B*) and RAD52-(1–192) (*C* and *D*) forms 10-nm diameter ring-shaped oligomers. Larger particles of wild-type RAD52 in *A* (also see Fig. 2) are not formed by RAD52-(1–192). Higher magnifications of both proteins reveal that the protrusions observed on the 10-nm rings of wild-type RAD52 are missing in the RAD52-(1–192) rings (*arrows* in *B* and *D*). *Black bars* = 0.05 μm in *A* and *C* and 0.01 μm in *B* and *D*.

namics 3.0 molecular weight calculator. Sum of squares errors less than 5000 were considered negligible.

Electron Microscopy—Proteins were prepared for EM by diluting wild-type or mutant RAD52 to 4.0 μM in a buffer containing 20 mM Tris-HCl, pH 7.5, 5% glycerol, 5 mM β-mercaptoethanol, 0.1 mM EDTA, and 100 mM KCl. Samples were spread onto thin carbon films on holey carbon grids (400 mesh), stained with 1% uranyl acetate, and visualized by transmission electron microscopy using a Philips CM10 microscope.

STEM Analysis—Analyses were carried out at the Brookhaven National Laboratory using unstained, unshadowed freeze-dried samples. Protein samples (~0.1 mg/ml) were applied to a thin carbon film supported by a thick holey film on titanium grids and freeze-dried overnight. The microscope operates at 40 kV. Operation of the STEM and data analyses were performed as described previously (23).

Gel Filtration—Samples of the RAD52-(218–418) protein at 1.2 mg/ml were loaded onto a Superdex 200 HR 10/30 gel filtration column (Amersham Pharmacia Biotech/LKB) equilibrated in buffer containing 20 mM MES, pH 6.0, 400 mM NaCl, 100 mM KCl, 10% (w/v) glycerol, 5 mM β-mercaptoethanol, and 1 mM EDTA. Analysis was performed using a BioLogic chromatography system (Bio-Rad) with an in-line UV detector.

RESULTS

Oligomeric Characteristics of RAD52 Proteins—EM analyses of wild-type RAD52 and RAD52-(1–192) show that both proteins form ring-shaped structures (Figs. 2 and 3). The average diameter of these particles, measured across the surface with the central pore, is 10 ± 1 nm, consistent with previous reports (9, 12, 21). Wild-type RAD52 also forms distinct larger particles that appear as various sized spheres and half-spheres ranging in diameter from 30 to 100 nm (Fig. 2). These particles consist of individual 10-nm rings as well as other less distinct com-

FIG. 4. **STEM histograms.** STEM mass analyses were performed as described under "Experimental Procedures." Histograms include pooled data from several separate analyses (eight for wild-type RAD52, six for RAD52-(1–192), and five for RAD52-(218–418)). Average mass values were as follows: A, wild-type RAD52 298 ± 69 kDa ($n = 309$); B, RAD52-(1–192) 227 ± 30 kDa ($n = 277$); C, RAD52-(218–418) 153 ± 40 kDa ($n = 119$).

TABLE I
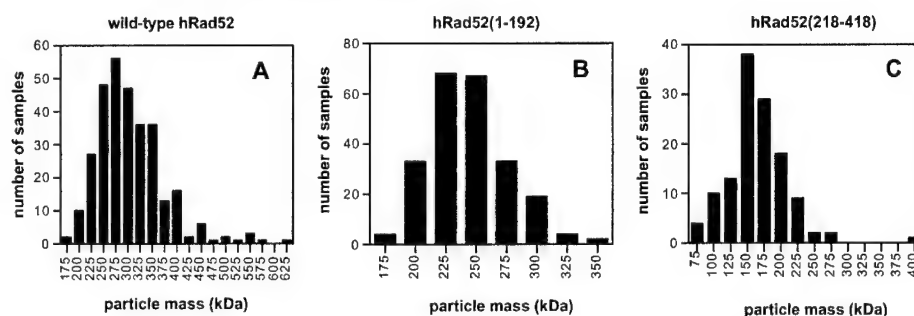*Dynamic light-scattering measurements of RAD52 proteins*

Protein	Concentration	Base line	Modality	SOS[a]	R_H[b]	Molecular mass	Peak[c] area
	mg/ml			*error*	*nm*	*kDa*	*%*
RAD52	3.5	1.007	Multimodal	3.10	6.6 (0.7)	279	10.5
					27.6 (9.3)	9.05×10^3	85.8
					711.0 (245)	2.40×10^7	3.7
RAD52-(1–192)	15	1.001	Monomodal	1.95	5.7 (1.2)	200	
RAD52-(218–418)	2	1.001	Monomodal	0.64	4.6 (2.1)	118	
Thioredoxin	1	1.001	Monomodal	3.3	2.0 (0.8)	14.8	

[a] SOS, sum of squares.
[b] Average hydrodynamic radius (R_H) is reported with the polydispersity (width of the distribution in nm) given in parentheses.
[c] For DynaLS results the percent peak area for the solvent peak is not reported.

pressed structures. For RAD52-(1–192) the majority of protein forms ring-shaped oligomers, and no larger particles were seen (Fig. 3). Even at increased concentrations (6 and 10 μM) RAD52-(1–192) shows no larger aggregates (data not shown). Higher magnifications reveal "protrusions" extending from the 10-nm rings formed by wild-type RAD52 that are missing in the 1–192 protein (see *arrows* in Fig. 3, *B* and *D*). These protrusions likely correspond to those modeled by Stasiak *et al.* (21), and our data show that they are part of the C-terminal portion of RAD52.

STEM analyses of wild-type RAD52 (2 μM) showed particle sizes ranging from 175 to 625 kDa with a mass average of 298 ± 69 kDa ($n = 309$; Fig. 4A). Given a molecular mass of 48 kDa for the His-tagged RAD52 protein, this range corresponds to particles that contain from 4 to 13 subunits with an average of six subunits. Similar analyses of the 1–192 protein showed particle sizes ranging from 100 to 350 kDa with a mass average of 227 ± 30 kDa ($n = 277$; Fig. 4B). For a monomer molecular mass of 23 kDa, this range corresponds to particles that contain from 4 to 15 subunits with an average of 10 subunits. Resolution of the ring-shaped oligomers in the electron micrographs was not high enough to count individual subunits, but our STEM data are consistent with previous work in which oligomeric rings of wild-type RAD52 were determined to be heptameric (21).

The oligomeric distribution of these proteins in solution was investigated by DLS. Wild-type RAD52 shows a multimodal profile with three peaks corresponding to particles with an average hydrodynamic radius of 6.6, 27.6, and 711.0 nm, respectively (Table I). These likely correspond to ring-shaped oligomers, the 30-nm particles described previously as "super-rings" (12) and seen in our micrographs (Fig. 2), and larger aggregates also observed in our micrographs. We find that the percent distribution of these various sized particles is effected by protein concentration, *i.e.* with increasing concentration the larger aggregates account for a larger percentage of the population. In contrast to wild type, RAD52-(1–192) shows a monomodal light-scattering profile that corresponds to a particle with a hydrodynamic radius of 6.1 nm (Table I), which is in agreement with our EM analysis.

The above analyses indicate at least two modes of RAD52 self-association that are experimentally separable, (i) forma-
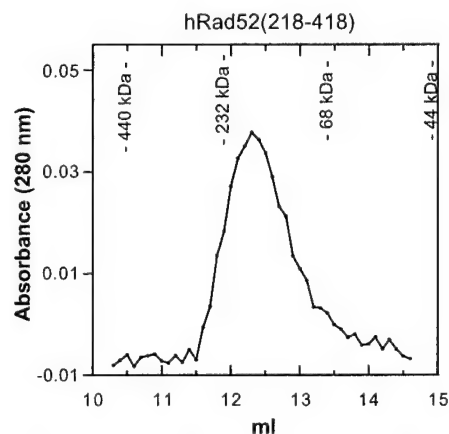

FIG. 5. **Gel filtration profile of the thioredoxin/218–418 fusion RAD52 protein.** The mutant protein (1.2 mg/ml, 35.8 μM) was loaded onto a Superdex 200 HR 10/30 gel filtration column, and elution of protein was followed at $A_{280 \text{ nm}}$. The indicated elution volumes of standards (ferritin, *440 kDa*; catalase, *232 kDa*; BSA, *68 kDa*; ovalbumin, *44 kDa*) were an average of four runs.

tion of ring-shaped oligomers and (ii) formation of larger aggregates. Because the latter seems to depend largely on the presence of residues C-terminal to position 192, we performed a number of assays to test for self-association on a mutant RAD52 containing only residues 218–418. Initial EM studies showed no distinct structural characteristics for this protein (data not shown), but STEM analysis revealed particle sizes ranging from 75 to 275 kDa (Fig. 4C) with a mass average of 153 ± 40 kDa ($n = 119$; Fig. 4C). Given a monomer molecular mass of 39 kDa, the particle composition ranges from two to seven subunits with an average of four subunits. Gel filtration shows a homogeneous peak corresponding to a molecular mass of 166 kDa (Fig. 5) and therefore to a particle containing approximately four subunits. Analysis by DLS shows a monomodal peak corresponding to a particle with an average R_H of 4.6 nm and a molecular mass of 118 kDa (therefore containing approximately three subunits). DLS measurements on thioredoxin alone show that it does not contribute to the oligomeric character of thioredoxin-RAD52-(218–418) (Table I). Together,

FIG. 6. **Gel-shift DNA Binding assays.** Indicated concentrations of either wild-type RAD52 or RAD52-(1–192) were incubated with a 5′-end-labeled 95-base oligonucleotide followed by cross-linking with glutaraldehyde as described under "Experimental Procedures." Reactions were electrophoresed on a 0.8% agarose gel. Radioactive material at the *top* of the gel represents protein-DNA complex trapped in the gel well. *u*, unbound DNA; *b*, protein-DNA complex.
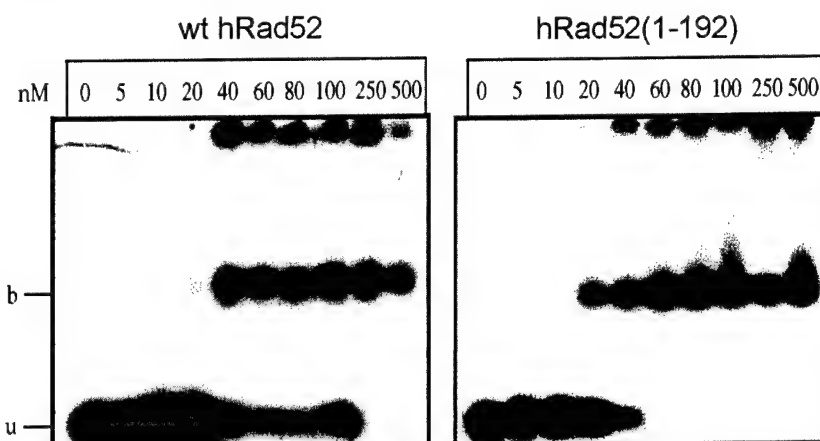
these data indicate that the C-terminal portion of RAD52 (residues 218–418) contains determinants of protein self-association that are distinct from those required to form 10-nm rings.

DNA Binding—Binding of wild-type RAD52 and RAD52-(1–192) to single-stranded DNA was analyzed by gel-shift assays. The gels in Fig. 6 are representative of five different experiments, each of which gave similar results. In each case, analysis of unbound and bound DNA (including that in the gel well) gave rise to a $K_{D(\text{app})}$ of 35 and 25 nM for wild-type RAD52 and RAD52-(1–192), respectively. This slight enhancement in binding affinity was observed consistently for RAD52-(1–192). With wild-type RAD52 a significant portion of bound DNA remained in the gel well, a result that likely reflects the ability of the wild-type protein to form greater amounts of self-aggregates than the 1–192 mutant protein (see below). Additionally, 100% of the DNA (2 nM total nucleotides) was bound by the 1–192 protein at 40–60 nM protein in the titration profile, whereas 100% binding by wild-type RAD52 consistently required greater than 100 nM protein. Assays using the RAD52-(218–418) mutant protein showed no DNA binding up to 2.0 μM protein (data not shown). These results show that the DNA binding domain of RAD52 is contained within the N-terminal portion of the protein and that removal of the C-terminal 227 residues results in a slight enhancement of DNA binding.

Interaction of RAD52 Proteins with RPA—Previous studies have mapped residues 221–280 as the domain in RAD52 that interacts with the 32-kDa subunit of RPA (16). To ensure that the 218–418 mutant construct maintained a native fold, we tested this protein for interaction with RPA using an immunoassay. Enzyme-linked immunosorbent assays showed that the 218–418 protein interacted with RPA with an affinity similar to that observed for wild-type RAD52 (Fig. 7). No interaction with RPA was observed for RAD52-(1–192), thioredoxin, or BSA.

DISCUSSION

Previous studies have shown that RAD52 exists in a number of oligomeric states ranging from rings with a 10-nm diameter to larger complexes with diameters of greater than 30 nm (9, 12, 20, 21). Recent observations indicate a direct role for these higher order protein-protein interactions in promoting DNA end-joining (20). We therefore sought to investigate the self-association properties of RAD52 utilizing an array of biophysical techniques.

In our EM studies of wild-type RAD52 and RAD52-(1–192), we observed ring structures with an average diameter of 10 ± 1 nm as has been reported previously (9, 12, 20, 21). Additionally, and as seen previously (12, 20, 21), we observed protrusions extending from wild-type RAD52 rings as well as a population of distinct larger particles. However, neither the protrusions nor the larger particles were observed with RAD52-(1–192). This suggests that
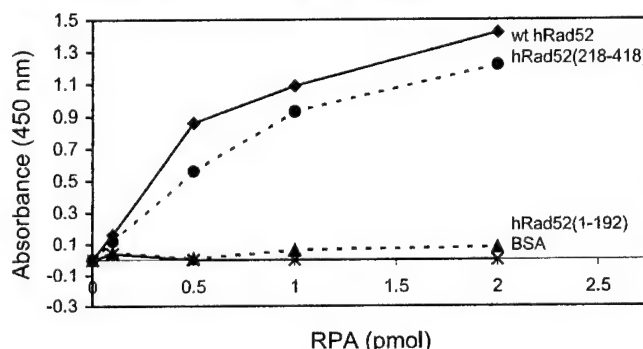
FIG. 7. **RAD52-RPA protein-protein interactions.** Enzyme-linked immunosorbent assays were performed as described under "Experimental Procedures" with RAD52 proteins immobilized to microtiter plates and probed with increasing amounts of RPA heterotrimer. The experiment was performed in triplicate, and the average for each RPA concentration was plotted. The error was on the order of 5–10%. *wt*, wild type.

residues within the C-terminal portion of the protein (residues 193–418) make up these protrusions and carry determinants for higher order RAD52 self-association.

DLS analysis of wild-type RAD52 and the two mutant proteins provides additional and complementary evidence for two distinct modes of RAD52 self-association. DLS analysis of wild-type RAD52 shows three peaks that likely correspond to the 10-nm ring-shaped oligomers and the 30-nm and larger particles observed by EM. In contrast, both RAD52-(1–192) and RAD52-(218–418) show a monomodal DLS profile indicating the presence of a single population of structures. The RAD52-(1–192) R_H is consistent with a ring structure, and the RAD52-(218–418) R_H indicates a complex composed of three subunits. This self-association of RAD52-(218–418) was confirmed by size-exclusion chromatography and STEM.

The ability of RAD52-(218–418) to self-associate was unexpected. Previous studies have suggested that residues 65–165 define the exclusive self-association domain in the RAD52 protein (18). Shen *et al.* (18) found that although N-terminal fragments of the protein self-associated in two-hybrid screens and affinity chromatography assays, fragments containing various portions of the C terminus, *e.g.* 287–418 or 166–418, did not. In contrast to these results, we find that RAD52-(218–418) is able to self-associate. Although our EM analysis revealed no distinct oligomeric structures for RAD52-(218–418), three different methods (STEM, gel filtration, and DLS) showed that this mutant formed oligomeric particles containing 3–4 subunits. These data for RAD52-(218–418), coupled with the inability of RAD52-(1–192) to form structures larger than the 10-nm rings, indicate that residues within the C-terminal region of the pro-

tein make important contributions to RAD52 self-association. Thus, the C-terminal region of RAD52 contains a novel self-association domain distinct from that previously identified within residues 65–165 (18).

Importantly, functional analyses of both the 1–192 and 218–418 mutant proteins show that each maintains an expected activity. Both wild-type RAD52 and the 1–192 proteins, which form ring-shaped oligomers, bound single-stranded DNA with similar affinities. This is consistent with previous studies that mapped the DNA binding domain of RAD52 to residues 39–80[2] (16). The elevated affinity of RAD52-(1–192) for single-stranded DNA was noted also for a similar Rad52p construct (24). Also as expected, RAD52-(218–418) showed a specific interaction with RPA. Again, this is consistent with previous studies that mapped the RPA interaction domain to residues 221–280 in RAD52 (16). The fact that both mutant proteins showed the expected functions demonstrates that they very likely maintain native structure, thereby supporting the relevance of differences observed in their oligomeric characteristics compared with wild-type RAD52.

In summary, our data support a model in which the self-association domain within the N-terminal region of RAD52 (residues 1–192) promotes the formation of ring-shaped oligomers that are functional for DNA binding, whereas the C-terminal domain (residues 218–418) mediates higher order self-association events. Additionally, the protrusions extending from the 10-nm ring structure of wild-type RAD52, originally modeled by Stasiak *et al.* (21) and seen clearly in our electron micrographs, correspond to the C-terminal region of the protein. Given the likely importance of higher order self-association to the ability of RAD52 to promote end-to-end joining of DNA breaks (20), these protrusions seem to mediate a critically important aspect of RAD52 function. Further studies of various mutant RAD52 proteins will clarify the contribution made by the different aspects of self-association toward the overall function of this important DNA repair protein.

REFERENCES

1. Game, J., and Mortimer, R. K. (1974) *Mutat. Res.* **24,** 281–292
2. Petes, T. D., Malone, R. E., and Symington, L. S. (1991) in *The Molecular and Cellular Biology of the Yeast, Saccharomyces* (Broach, J. R., Pringle, J. R., and Jones, E. W., eds) pp. 407–522, Cold Spring Harbor Laboratory Press, Cold Spring Harbor, NY
3. Shinohara, A., and Ogawa, T. (1998) *Nature* **391,** 404–407
4. Milne, G. T., and Weaver, D. T. (1993) *Genes Dev.* **7,** 1755–1765
5. Hays, S. L., Firmenich, A. A., and Berg, P. (1995) *Proc. Natl. Acad. Sci., U. S. A.* **92,** 6925–6929
6. Johnson, R. D., and Symington, L. S. (1995) *Mol. Cell. Biol.* **15,** 4843–4850
7. Sung, P. (1997) *J. Biol. Chem.* **272,** 28194–28197
8. New, J. H., Sugiyama, T., Zaitseva, E., and Kowalczykowski, S. C. (1998) *Nature* **391,** 407–410
9. Shinohara, A., Shinohara, M., Ohta, T., Matsuda, S., and Ogawa, T. (1998) *Genes Cells* **3,** 145–156
10. Sugiyama, T., New, J. H., and Kowalczykowski, S. C. (1998) *Proc. Natl. Acad. Sci. U. S. A.* **95,** 6049–6054
11. Wold, M. S. (1997) *Annu. Rev. Biochem.* **66,** 61–91
12. Van Dyck, E., Hajibagheri, N. M. A., Stasiak, A., and West, S. C. (1998) *J. Mol. Biol.* **284,** 1027–1038
13. Golub, E. I., Gupta, R. C., Haaf, T., Wold, M. S., and Radding, C. M. (1998) *Nucleic Acids Res.* **26,** 5388–5393
14. Baumann, P., and West, S. C. (1999) *J. Mol. Biol.* **291,** 363–374
15. Shen, Z., Cloud, K. G., Chen, D. J., and Park, M. S. (1996) *J. Biol. Chem.* **271,** 148–152
16. Park, M. S., Ludwig, D. L., Stigger, E., and Lee, S. H. (1996) *J. Biol. Chem.* **271,** 18996–19000
17. Benson, F. E., Baumann, P., and West, S. C. (1998) *Nature* **391,** 401–404
18. Shen, Z., Peterson, S. R., Comeaux, J. C., Zastrow, D., Moyzis, R. K., Bradbury, E. M., and Chen, D. J. (1996) *Mutat. Res.* **364,** 81–89
19. Kito, K., Wada, H., Yeh, E. T., and Kamitani, T. (1999) *Biochim. Biophys. Acta* **1489,** 303–314
20. Van Dyck, E., Stasiak, A. Z., Stasiak, A., and West, S. C. (1999) *Nature* **398,** 728–731
21. Stasiak, A. Z., Larquet, E., Stasiak, A., Muller, S., Engel, A., Dyck, E. V., West, S. C., and Egelman, E. H. (2000) *Curr. Biol.* **10,** 337–340
22. Henricksen, L. A., Umbricht, C. B., and Wold, M. S. (1994) *J. Biol. Chem.* **269,** 11121–11132
23. Wall, J. S., Hainfeld, J. F., and Simon, M. N. (1998) *Methods Cell Biol.* **53,** 139–164
24. Mortensen, U. H., Bendixen, C., Sunjevaric, I., and Rothstein, R. (1996) *Proc. Natl. Acad. Sci. U. S. A.* **93,** 10729–10734

research papers

**Jeff E. Habel, Jeffrey F. Ohren
and Gloria E. O. Borgstahl***

University of Toledo, Department of Chemistry,
2801 West Bancroft Street, Toledo, OH 43606,
USA

Correspondence e-mail:
gborgst@uoft02.utoledo.edu

Dynamic light-scattering analysis of full-length human RPA14/32 dimer: purification, crystallization and self-association

Replication protein A (RPA) is a single-stranded DNA-binding protein involved in all aspects of eukaryotic DNA metabolism. A soluble heterodimeric form of RPA is composed of 14 and 32 kDa subunits (RPA14/32). Dynamic light-scattering (DLS) analysis was used to improve the purification, stabilization and crystallization of RPA14/32. Increasing the concentration of reducing agent in the last stage of purification diminished the size of a secondary peak in the anion-exchange chromatograph and promoted a single species in solution. This resulted in decreased polydispersity in the purified protein and enhanced the crystallization time from 9–12 months to 6 d. With this homogeneous preparation, the reversible association of RPA14/32 into a dimer of dimers was demonstrated by DLS. Four different crystal forms of RPA14/32 were obtained for structure determination and complete diffraction data were collected using synchrotron radiation for three of them. Data to 2.4 Å resolution was collected from hexagonal crystals ($P3_2$ or $P3_1$; $a = b = 63.0$, $c = 272.6$ Å) and to 2.2 and 1.9 Å resolution from two orthorhombic crystal forms (both $P2_12_12_1$; form I, $a = 61.4$, $b = 75.2$, $c = 131.6$ Å; form II, $a = 81.8$, $b = 140.4$, $c = 173.1$ Å).

1. Introduction

Replication protein A (RPA) is a single-stranded DNA-binding protein that has been implicated in all aspects of eukaryotic DNA metabolism, including replication, transcription, recombination and repair (for reviews, see Wold, 1997; Iftode *et al.*, 1999). The three subunits of RPA are designated RPA14, RPA32 and RPA70 according to their apparent molecular weights. RPA70 contains the primary ssDNA-binding site and interacts with several proteins, including P53 (Dutta *et al.*, 1993; He *et al.*, 1993; Li & Botchan, 1993) and XPA (Lee & Kim, 1995; Li *et al.*, 1995; Matsuda *et al.*, 1995). RPA32 is phosphorylated in a cell-cycle-dependent manner (Din *et al.*, 1990; Fang & Newport, 1993) during apoptosis (Treuner *et al.*, 1999) and in response to UV light (Carty *et al.*, 1994) and ionizing radiation (Liu & Weaver, 1993; Boubnov & Weaver, 1995; Fried *et al.*, 1996). *In vitro*, RPA32 is phosphorylated by ATM kinase (Gately *et al.*, 1998), cdc2 kinase (Dutta & Stillman, 1992) and DNA-dependent protein kinase (Brush *et al.*, 1994; Boubnov & Weaver, 1995). RPA32 contains a weak ssDNA-binding site (Bochkareva *et al.*, 1998) and its C-terminal domain interacts with several proteins, including RAD52 (Park *et al.*, 1996) and XPA. RPA14 plays a structural role in heterotrimer assembly and stability (Henricksen *et al.*, 1994). RPA is known to exist in two soluble forms: the heterotrimer and the RPA14/32 heterodimer

(Henricksen *et al.*, 1994). The RPA heterotrimer is extremely stable (Fairman & Stillman, 1988; Wold & Kelly, 1988; Brill & Stillman, 1991) and its roles in DNA metabolism are well known. Interestingly, the separation of the RPA14/32 dimer from RPA70 is promoted by hyperphosphorylation of RPA32 both *in vitro* (Treuner, Findeisen *et al.*, 1999) and in cells undergoing apoptosis (Treuner, Okuyama *et al.*, 1999). These studies suggest a physiological role for the RPA14/32 dimer.

Owing to the multidimensional role RPA plays in DNA metabolism, it is of great interest to understand the structure in atomic detail. An NMR solution structure of the N-terminal RPA70 domain (Jacobs *et al.*, 1999) and crystal structures at moderate resolution of proteolytic core fragments of RPA70 (Bochkarev *et al.*, 1997) and RPA14/32 (Bochkarev *et al.*, 1999) have been reported. Unfortunately, the intact full-length holoenzyme is very difficult to purify and structural data remain elusive. Here, we demonstrate the utility of using dynamic light-scattering (DLS) analysis in improving the purification, stabilization and crystallization of full-length recombinant human RPA14/32 dimer. Complete diffraction data from orthorhombic and hexagonal crystals are reported.

2. Experimental

2.1. Expression and purification

RPA14 and RPA32 subunits were co-expressed from a single pET16 plasmid (Novagen). A 6×His tag followed by a thrombin cleavage site was placed at the N-terminus of RPA14. BL21(DE3) cells (Novagen) were transformed and 8 l of Terrific Broth containing $100 \mu g \, ml^{-1}$ ampicillin was inoculated with an 8 ml starter culture and rested at room temperature overnight in a laboratory fermentor (Virtis). The next morning the culture was grown ($300 \, rev \, min^{-1}$, 310 K, $15 \, l \, O_2 \, min^{-1}$) to an OD_{600} of 4.0–5.0 (4.5–5 h), induced with $1 \, mM$ IPTG and grown for another 3.5–4 h. The cells were harvested by centrifugation ($10\,000 \, rev \, min^{-1}$, 277 K, 10 min) and the cell pellet was resuspended in four volumes of lysis buffer ($30 \, mM$ HEPES pH 7.8, $200 \, mM$ KCl) supplemented with 4–10 mM imidazole and $1 \, mM$ DTT.

For preparation *A*, the cells were lysed by sonication, centrifuged ($15\,000 \, rev \, min^{-1}$, 277 K, 30 min) and the supernatant was passed through a 0.20 µm filter. The clarified lysate was loaded onto a $1.67 \, ml \, MC/M \, Ni^{2+}$ affinity column (PerSeptive Biosystems) equilibrated with lysis buffer with $4 \, mM$ imidazole. The column was washed with 15 column volumes (CV) of lysis buffer with $60 \, mM$ imidazole and the protein eluted with a 60–1000 mM, 20 CV imidazole gradient using the BioCAD Sprint. For preparations *B–G*, the cells were lysed by three passes through a French pressure cell (SLM-Aminco). The lysed cells were centrifuged and supernatant was passed through 5–10 ml of Cellular Debris Remover resin (Whatman) in a 60 ml syringe. The clarified lysate was loaded onto a 5 ml Ni-NTA Superflow column (Qiagen) equilibrated with lysis buffer with $10 \, mM$ imidazole. The column was washed with 10 CV of lysis buffer with $10 \, mM$ imidazole and the protein was eluted with a 10–500 mM 20 CV

Table 1
Interpretation and use of the statistical parameters calculated by *Dynamics* 4.0.

Parameter	Interpretation†
Baseline	
0.977–1.002	Monomodal distribution
1.003–1.005	Bimodal distribution, use *DynaLS*
>1.005	Bimodal/multimodal distribution, use *DynaLS*
Sum of squares (SOS)	
1.000–5.000	Low noise, negligible error
5.000–20.000	Background error owing to noise, low protein concentration or a small amount of polydispersity
>20.000	High noise/error owing to high polydispersity in size distribution (aggregation), irregular solvent
Polydispersity	Note: this parameter should be used for monomodal distributions only
$C_P/R_{II} < 15\%$	Monodisperse solution, very likely to crystallize
$C_P/R_{II} < 30\%$	A moderate amount of polydispersity, more likely to crystallize
$C_P/R_{II} > 30\%$	A significant amount of polydispersity, less likely to crystallize

† Adapted from the DynaPro-801 Operator Manual, Protein Solutions Inc.

imidazole gradient using a Bio-Logic LP system (Bio-Rad). For preparations *A–G*, the pooled fractions were diluted five times with $30 \, mM$ HEPES pH 7.8 and varying amounts of fresh DTT was added. The diluted protein was loaded onto a 1.67 ml POROS HQ/M strong anion-exchange column (PerSeptive Biosystems). The column was washed with 10 CV of $30 \, mM$ HEPES pH 7.8 containing DTT and $10 \, mM$ KCl. For preparation *A*, the protein was eluted with a 10–1000 mM KCl 10 CV gradient. For preparations *B–G*, a gradient from 10–700 mM KCl over 40 CV was used. All column fractions were analyzed by SDS–PAGE (Pharmacia LKB PhastSystem) and those HQ column fractions of sufficient concentration were also analyzed by DLS. Pooled fractions were concentrated with a Centriprep YM-10 (Amicon). Protein concentration was determined using the Bradford Protein Assay (BioRAD) with BSA as the standard.

2.2. Dynamic light-scattering analysis

DLS was carried out using a DynaPro-801 molecular-sizing instrument equipped with a microsampler (Protein Solutions). A 50 µl sample was passed through a filtering assembly containing a 0.02 µm filter into a 12 µl chamber quartz cuvette. The data were analyzed using the *Dynamics* 4.0 and *DynaLS* software as described by Moradian-Oldak *et al.* (1998). Interpretation of the statistical parameters generated by the *Dynamics* 4.0 software is summarized in Table 1.

2.3. Crystallization

All crystallization was performed at 293 K using vapor-diffusion methods with hanging or sitting drops. Drop volumes of 4 µl (by mixing equal volumes of protein and reservoir solutions) and reservoir volumes of 500 µl were used. Initial screening was performed with Hampton Research Crystal Screens 1 and 2 (Jancarik & Kim, 1991).

Table 2
Dynamic light-scattering data and resultant crystallization time.

Data with a monomodal distribution was analyzed using *Dynamics* 4.0 and multimodal data with *DynaLS*, with percentages of peak area given in parentheses. The concentration of DTT used in the HQ buffer system is given. Crystallization condition I was used for each preparation and monitored weekly.

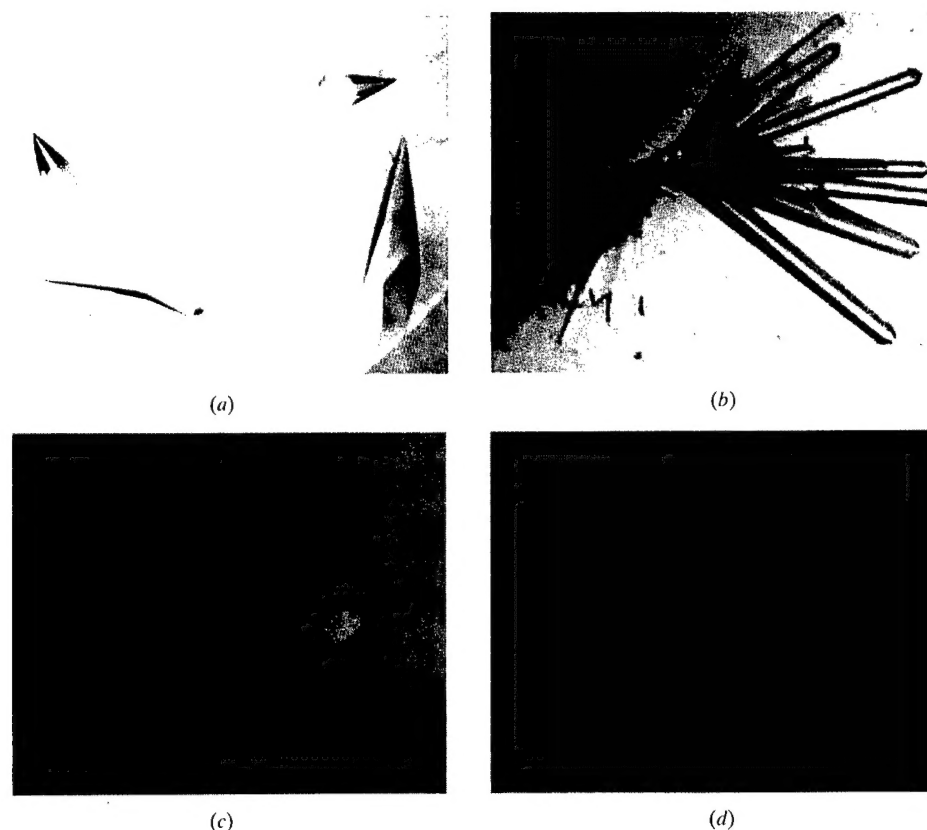| Preparation	Concentration (mg ml^{-1})	R_H (nm)	MW (kDa)	C_P (nm)	C_P/R_H (%)	Baseline	SOS error	DTT (mM)	Time (d)
A	5	3.1 (77) 1090 (23)	45.0	NA	NA	1.047	1.400	0	270–360
B	1–2	3.41	56.8	1.1	33.1	1.001	6.065	0	28
C	1–2	3.39	56.0	0.9	25.7	1.000	4.550	1	28
D	1–2	3.49	59.9	0.7	20.8	1.001	1.397	5	14
E	10	3.39	56.1	0.6	18.3	1.000	1.363	10	6
F	10	3.60	64.9	0.6	17.5	1.000	0.848	10	6
G	13	4.13	90.3	0.6	14.5	1.000	0.666	10	NA

2.4. Data collection

Single crystals were immersed in cryoprotectant (either the reservoir solution with 30% glycerol or paratone-N oil) for 3 s, mounted in a cryoloop and immediately placed in a 100 K nitrogen-gas stream. Diffraction data were collected on hexagonal (Fig. 1a) and orthorhombic crystal form II (Fig. 1d) at Stanford Synchrotron Radiation Laboratory beamline 7-1 with a MAR345 detector at a wavelength of 1.08 Å. Low-resolution (LR) and high-resolution (HR) passes were designed using *MOSFLM/STRATEGY*. For hexagonal crystals, 28 HR images were collected at a crystal-to-detector distance (XTD) of 300 mm, $\Delta\varphi = 2°$ using the 345 mm plate (edge = 2.09 Å), 30 LR images were collected at an XTD of 350 mm and 58 LR images were collected at an XTD of 300 mm using the 180 mm plate (edge = 3.72–4.3 Å). For orthorhombic form II crystals, 365 HR images were collected at an XTD of 225 mm, $\Delta\varphi = 0.25°$ (0.5° for 20 images) using the 300 mm plate (edge = 1.86 Å) and 366 LR images were collected at an XTD of 240 mm, $\Delta\varphi = 0.5°$ (1.0° for 48 images) using the 180 mm plate (edge = 3.03 Å). Images were integrated with *MOSFLM* (Powell, 1999) and scaled using *SCALA* and the *CCP4i* graphical interface (Collaborative Computational Project, Number 4, 1994). The HR data from the orthorhombic crystals were difficult to integrate because all the data were recorded as partial reflections. A pre-release of a new version of *MOSFLM* was provided by Dr Harry Powell to integrate these images using the POSTREF MULTI keyword.

Diffraction data were collected from orthorhombic crystal form I (Fig. 1c) at beamline 17-ID in the facilities of the Industrial Macromolecular Crystallography Association Collaborative Access Team (IMCA-CAT) at the Advanced Photon Source (APS). 180 images were collected at a crystal-to-detector distance of 120 mm with $\Delta\varphi = 1°$, $\lambda = 1.2$ Å and using the MARCCD detector. Data were processed using the *HKL*2000 program suite (Otwinowski & Minor, 1996).

(a)   (b)   (c)   (d)

Figure 1
Crystals of RPA14/32. (a) Hexagonal crystals grown from preparation A with a precipitating solution of 0.1 M bicine pH 9.0, 10% acetonitrile and 20% saturated ammonium sulfate. The largest crystal was 90 × 150 μm. (b) Monoclinic crystals grown from preparation E with 10% dioxane, 0.1 M MES pH 6.5 and 37% saturated ammonium sulfate. The largest crystal was 44 × 440 μm. (c) Orthorhombic crystal form I grown from preparation P1 with 0.1 M MES pH 6.3, 5% saturated ammonium sulfate and 26% PEG MME 5000 (242 × 275 μm). (d) Orthorhombic crystal form II grown from preparation P1 with 10% dioxane, 0.1 M MES pH 6.5 and 39% saturated ammonium sulfate (132 × 220 μm).

3. Results and discussion

RPA14/32 was overexpressed in *Escherichia coli* and up to 15 mg of pure protein was obtained from a liter of culture. Since monodispersity is thought to be predictive of crystallizability (Zulauf & D'Arcy, 1992; Ferre-D'Amare & Burley, 1997), DLS was used to examine all preparations of RPA14/32. Initial

purifications were multimodal (baseline 1.047) and polydisperse (Table 2, preparation A) and did not crystallize unless organics were added to the crystallization setup. After 9–12 months, hexagonal crystals grew from solutions that contained 20–30% saturated ammonium sulfate, 0.1 M HEPES, Tris or bicine pH 7–9 and 6–10% organic solvent (acetonitrile, 2-propanol or methanol). Although of diffraction quality, these crystals were difficult to reproduce (Fig. 1a).

Preparation B was monomodal (baseline 1.001, Table 2) but was significantly polydisperse ($C_P/R_H = 33.1$). Initial crystallization screens produced microcrystals within a month. Grid-screen optimization resulted in the following crystallization condition that produced monoclinic diffraction-quality crystals (Fig. 1b): 10% dioxane, 0.1 M MES pH 5.7–6.5 and 34–41% saturated ammonium sulfate (condition I). Prepara-

Table 3
Dynamic light-scattering data for chromatography peaks P and $P1$.

Preparation	Concentration (mg ml^{-1})	R_H (nm)	MW (kDa)	C_P (nm)	C_P/R_H (%)	Baseline error	SOS
P	8.2	4.12	89.7	0.9	22.8	1.001	1.201
$P1$	8.5	3.62	65.5	0.9	23.7	1.001	1.431
$P + P1$	8.35	3.9 (91) 1170 (6.6)	78.5	NA	NA	1.005	2.841
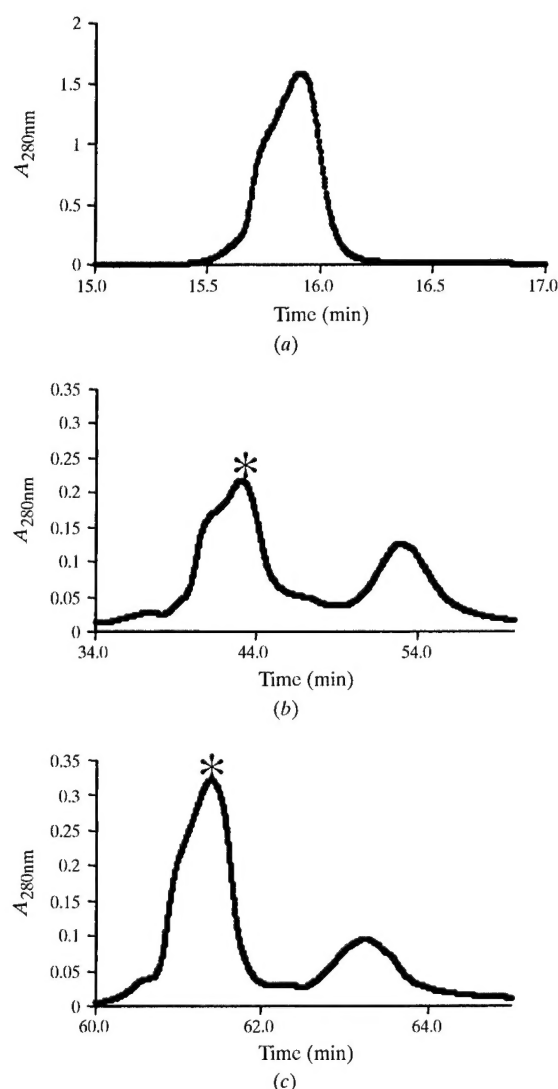
Figure 2
Representative chromatograms of RPA14/32 elution at ~300 mM KCl from the HQ anion-exchange column. (a) Preparation A, (b) preparation B, (c) preparation C. SDS–PAGE analysis showed that all peaks are composed of hRPA14/32 dimer (data not shown). For preparations B–G, the fractions corresponding to the peak indicated with an asterisk (*) were collected.

tion B was significantly less polydisperse and crystallized in less time than preparation A. The differences between these preparations, the lysis method and the type of nickel affinity matrix used, do not account for the overall improvement in polydispersity. The elution profiles from the HQ anion-exchange column (Figs. 2a and 2b) show that in preparation B, where a shallower salt gradient was used, two peaks were separated, whereas in preparation A the protein eluted as one peak. In both preparations, analysis by SDS–PAGE indicated that all the peaks contained only RPA14/32. The lack of separation of these peaks in preparation A probably contributed greatly to the polydispersity of the early RPA14/32 samples (see below).

The primary sequence of RPA14/32 contains four cysteine residues (two in each subunit) and the structure of the proteolytic core of RPA14/32 had free cysteines (Bochkarev et al., 1999). These observations suggested the need for a reducing environment during protein purification. The effect of varying the concentration of dithiothreitol (DTT) in the HQ buffer system was monitored by DLS and crystallization time. In preparations B–G, as the DTT concentration was increased, polydispersity (C_P/R_H) and the time for crystal formation systematically decreased (Table 2). A DTT effect was also seen in the elution profiles. When fresh 1 mM DTT was added during the dilution of the protein sample and added to the HQ buffer system, the first peak increased and the second peak decreased (Figs. 2b and 2c). With 10 mM DTT, the second peak nearly disappears (data not shown). This suggests that the reduction of disulfide bond(s) is involved in converting the second peak into the first peak.

As frequently happens in science, an interesting observation on RPA14/32 came from careful analysis of a fortuitous mistake. Early in this work, the ionic strength of the protein sample was not reduced by dilution before loading onto the HQ column. The standard HQ protocol was run and a fraction of the protein sample was found to bind to the column (fraction P, Table 2). The flowthrough from this column was then diluted and reloaded onto the HQ column. The protein fraction $P1$ was eluted from the column. When analyzed by DLS (Table 3), fractions P and $P1$ were monomodal (baseline 1.001) with moderate polydispersity (C_P/R_H 23%). However, when the two fractions were mixed together, the solution became multimodal (baseline 1.005) with 7% high-molecular-weight aggregates. The molecular weight of fraction P (90 kDa) corresponded to that of a dimer of dimers, whereas fraction $P1$ was closer to that of a single dimer.

research papers

Table 4
Dynamic light-scattering data collected at various time points after the addition of acetonitrile to $P + P1$ mixture.

Time (h)	R_H (nm)	MW (kDa)	Baseline error	SOS
0	3.61 (77.5) 1340 (8.7)	65.1	1.010	1.837
1	3.84 (94.4) 1310 (4.4)	75.6	1.003	1.539
3	4.02 (96.4) 1270 (1.9)	84.5	1.001	1.459

Table 5
Dynamic light-scattering data on the dilution of preparation G.

Line No.	Concentration (mg ml^{-1})	R_H (nm)	MW (kDa)	C_P (nm)	C_P/R_H (%)	Baseline error	SOS
1	13	4.13	90.3	0.6	14.5	1.000	0.677
2	6.5	3.52 (77.7) 30.1 (3.3) 986 (18.3)	61.2 11200	NA	NA	1.022	5.211
3	6.5	3.52 (87.4) 1330 (6.7)	61.2	NA	NA	1.005	0.881
4	6.5	3.69	68.5	0.6	16.6	1.000	0.522

Crystallization conditions were screened and optimized for preparation $P1$. Large chunky crystals (Fig. 1c) were obtained from solutions containing 0–5% saturated ammonium sulfate, 0.1 M MES pH 5.9–6.5 and 16–36% PEG MME 5000 (condition II). These crystals were extremely sensitive and cracked easily when cryoprotected with glycerol. Diffraction data of reasonable quality was obtained using paratone-N oil as a cryoprotectant. Preparations B–G will not crystallize under condition II but preparation $P1$ will crystallize under condition I in an orthorhombic space group (Fig. 1d).

The different oligomerization state of the protein fractions P and $P1$ may explain the multimodality and polydispersity of preparation A. Since crystals were obtained when 6–10% organic solvent was added to preparation A, it was postulated that acetonitrile would reduce the polydispersity of the $P + P1$ mixture. Acetonitrile was added to the $P + P1$ mixture to a final concentration of 6%, incubated at 277 K for 3 h and monitored periodically by DLS (Table 4). Incubation with acetonitrile caused the amount of non-aggregated RPA14/32 to increase from 78 to 96% and the solution becomes monomodal. Interestingly, the molecular weight of the non-aggregated species continues to increase until it is roughly the size of a dimer of dimers.

It was noted that as the protein concentration increased, the molecular weight increased (Table 2) and at 13 mg ml^{-1} (preparation G) it was consistent with a dimer of dimers in solution. Therefore, this apparent self-association of the dimer was analyzed by dilution followed by DLS. Samples of preparation G (Table 5, row 1) were diluted with an equal volume of the following buffers: 30 mM HEPES pH 7.8 buffer (row 2), 30 mM HEPES pH 7.8 and 200 mM KCl (row 3) or 30 mM HEPES pH 7.8, 200 mM KCl and 10 mM DTT (row 4). Dilution with buffer alone produced a smaller molecular

Table 6
Data-collection statistics.

	Orthorhombic form I	Orthorhombic form II	Hexagonal
Beamline	APS 17-ID	SSRL 7-1	SSRL 7-1
Detector	MAR CCD	MAR345	MAR345
Temperature (K)	100	100	100
Wavelength (Å)	1.2	1.08	1.08
Space group	$P2_12_12_1$	$P2_12_12_1$	$P3_2$ (or $P3_1$)
Unit-cell parameters (Å)	$a = 61.4$, $b = 75.2$, $c = 131.7$	$a = 81.8$, $b = 140.4$, $c = 173.1$	$a = b = 63.0$, $c = 272.6$
Heterodimers in the asymmetric unit	1	3–5	2–3
V_M (Å^3 Da^{-1})	3.17	3.42–2.05	3.25–2.17
Solvent content (%)	61	64–40	62–43
Resolution (Å)	2.20	1.86	2.40
No. of measured reflections	181370	820454	141010
No. of unique reflections	31207	158549	43885
Completeness (%)	98.2 (97.9)	95.6 (81.4)	92.7 (91.9)
$I/\sigma(I)$	18.3 (2.5)	9.3 (1.0)	4.5 (1.0)
Multiplicity	5.8	5.2 (3.3)	3.2 (2.0)
R_{merge}† (%)	8.9	6.0	11.7

† $R_{merge} = \sum_{hkl}|\langle I_{hkl}\rangle - I_{hkl}|/\sum_{hkl}I_{hkl}$.

weight species in addition to large aggregates. Dilution with buffer and salt also produced large-molecular-weight aggregates, but more of the protein sample remains as the single dimer as indicated by an increase in the peak area (from 78 to 87%) associated with the 61 kDa species. Addition of DTT produced a monomodal solution and completely disrupted the large-molecular-weight aggregates. Therefore, the large aggregates of RPA14/32 are probably a consequence of inappropriate disulfide-bond formation and the dimer of dimers appears to be a reversible association. The physiological roles of the RPA14/32 dimer of dimers and the solvent-accessible cysteines on the surface of the molecule are unknown. The possibility of a RPA14/32 dimer of dimers was also suggested by Bochkarev *et al.* (1999).

Three complete sets of cryocooled synchrotron diffraction data have been collected for structure determination (Table 6). Space groups were assigned by autoindexing, comparing R_{merge} values for space groups within the indicated Laue group and by observed systematic absences. The hexagonal crystals (Fig. 1a) diffracted to 2.4 Å resolution, with space group $P3_2$ (or $P3_1$) and unit-cell parameters $a = b = 63.0$, $c = 272.6$ Å. The orthorhombic crystal form I (Fig. 1c) diffracted to 2.2 Å resolution, with space group $P2_12_12_1$ and unit-cell parameters $a = 61.4$, $b = 75.2$, $c = 131.7$ Å. The orthorhombic crystal form II (Fig. 1d) diffracted to 1.9 Å resolution with space group $P2_12_12_1$ and unit-cell parameters $a = 81.8$, $b = 140.4$, $c = 173.1$ Å. Interestingly, solvent-content analysis (Matthews, 1968) indicates several heterodimers in the asymmetric unit of the orthorhombic crystal form II and hexagonal unit cells. Solution of the phase problem using coordinates of a proteolytic fragment of RPA14/32 (containing intact RPA14 and 60% of RPA32; PDB code 1quq) is in progress.

References

Bochkarev, A., Bochkareva, E., Frappier, L. & Edwards, A. M. (1999). *EMBO J.* **18**, 4498–4504.

Bochkarev, A., Pfuetzner, R. A., Edwards, A. M. & Frappier, L. (1997). *Nature (London)*, **385**, 176–181.

Bochkareva, E., Frappier, L., Edwards, A. M. & Bochkarev, A. (1998). *J. Biol. Chem.* **273**, 3932–3936.

Boubnov, N. V. & Weaver, D. T. (1995). *Mol. Cell. Biol.* **15**, 5700–5706.

Brill, S. J. & Stillman, B. (1991). *Genes Dev.* **5**, 1589–1600.

Brush, G. S., Anderson, C. W. & Kelly, T. J. (1994). *Proc. Natl Acad. Sci. USA*, **91**, 12520–12524.

Carty, M. P., Zernik-Kobak, M., McGrath, S. & Dixon, K. (1994). *EMBO J.* **13**, 2114–2123.

Collaborative Computational Project, Number 4 (1994). *Acta Cryst.* D**50**, 760–763.

Din, S.-U., Brill, S. J., Fairman, M. P. & Stillman, B. (1990). *Genes Dev.* **4**, 968–977.

Dutta, A., Ruppert, J. M., Aster, J. C. & Winchester, E. (1993). *Nature (London)*, **365**, 79–82.

Dutta, A. & Stillman, B. (1992). *EMBO J.* **11**, 2189–2199.

Fairman, M. P. & Stillman, B. (1988). *EMBO J.* **7**, 1211–1218.

Fang, F. & Newport, J. W. (1993). *J. Cell Sci.* **106**, 983–994.

Ferre-D'Amare, A. R. & Burley, S. K. (1997). *Methods Enzymol.* **276**, 157–166.

Fried, L. M., Koumenis, C., Peterson, S. R., Green, S. L., Zijl, P. V., Turner, J. A., Chen, D. J., Fishel, R., Giaccia, A. J., Brown, J. M. & Kirchgessner, C. U. (1996). *Proc. Natl Acad. Sci. USA*, **93**, 13825–13830.

Gately, D. P., Hittle, J. C., Chan, G. K. T. & Yen, T. J. (1998). *Mol. Biol. Cell*, **9**, 2361–2374.

He, Z., Brinton, B. T., Greenblatt, J., Hassell, J. A. & Ingles, C. J. (1993). *Cell*, **73**, 1223–1232.

Henricksen, L. A., Umbricht, C. B. & Wold, M. S. (1994). *J. Biol. Chem.* **269**, 11121–11132.

Iftode, C., Daniely, Y. & Borowiec, J. A. (1999). *Crit. Rev. Biochem. Mol. Biol.* **34**, 141–180.

Jacobs, D. M., Lipton, A. S., Isern, N. G., Daughdrill, G. W., Lowry, D. F., Gomes, X. & Wold, M. S. (1999). *J. Biomol. NMR*, **14**, 321–331.

Jancarik, J. & Kim, S.-H. (1991). *J. Appl. Cryst.* **24**, 409–411.

Lee, S. H. & Kim, D. K. (1995). *J. Biol. Chem.* **270**, 12801–12807.

Li, L., Lu, X., Peterson, C. A. & Legerski, R. J. (1995). *Mol. Cell. Biol.* **15**, 5396–5402.

Li, R. & Botchan, M. R. (1993). *Cell*, **73**, 1207–1221.

Liu, V. F. & Weaver, D. T. (1993). *Mol. Cell. Biol.* **13**, 7222–7231.

Matsuda, T., Saijo, M., Kuraoka, I., Kobayashi, T., Nakatsu, Y., Nagai, A., Enjoji, T., Masutani, C., Sugasawa, K., Hanaoka, F., Yasui, A. & Tanaka, K. (1995). *J. Biol. Chem.* **270**, 4152–4157.

Matthews, B. W. (1968). *J. Mol. Biol.* **33**, 491–497.

Moradian-Oldak, J., Leung, W. & Fincham, A. G. (1998). *J. Struct. Biol.* **122**, 320–327.

Otwinowski, Z. & Minor, W. (1996). *Methods Enzymol.* **276**, 307–326.

Park, M. S., Ludwig, D. L., Stigger, E. & Lee, S. H. (1996). *J. Biol. Chem.* **271**, 18996–19000.

Powell, H. R. (1999). *Acta Cryst.* D**55**, 1690–1695.

Treuner, K., Findeisen, M., Strausfeld, U. & Knippers, R. (1999). *J. Biol. Chem.* **274**, 15556–15561.

Treuner, K., Okuyama, A., Knippers, R. & Fackelmayer, F. O. (1999). *Nucleic Acids Res.* **27**, 1499–1504.

Wold, M. S. (1997). *Annu. Rev. Biochem.* **66**, 61–91.

Wold, M. S. & Kelly, T. (1988). *Proc. Natl Acad. Sci. USA*, **85**, 2523–2527.

Zulauf, M. & D'Arcy, A. (1992). *J. Cryst. Growth*, **122**, 102–106.